Bonding Probabilities in Cold Spray Deposition of Composite Blends

Authors:

ERNST, Kerstin Raffaela [a]

ERNST, Thomas Michael [b]

GÄRTNER, Frank [a]

ASSADI, Hamid [c]

KLASSEN, Thomas [a]

Affiliations:

[a] Institute of Materials Technology, Helmut-Schmidt-University/University of the Federal Armed Forces Hamburg, 22043 Hamburg, Germany

[b] Department for Neurology, University Hospital Essen, University of Duisburg Essen, 45147 Essen, Germany

[c] Brunel Centre for Advanced Solidification Technology, Brunel University London, Uxbridge UB8 3PH, Great Britain

Corresponding authors:

Frank Gärtner, frank.gaertner@hsu-hh.de, Institute of Materials Technology, Helmut-Schmidt-University/University of the Federal Armed Forces Hamburg, 22043 Hamburg, Germany

Kerstin Raffaela Ernst, Kerstin_Ernst@mail.de

Abstract

Cold gas spraying of metal alloys using single feedstock powder is well described in terms of impact conditions and critical velocities for bonding of similar particles. In contrast, the mechanism of layer build-up in cold spraying of dissimilar powder blends, especially where the particles have significantly different thermomechanical properties, is far from being fully established and has remained an open question.

We explore this question by taking W-Cu and Mo-Cu as example blends of significantly dissimilar materials, with potential applications in thermal management systems. The current study aims mainly to provide a comprehensive overview of the electrical, mechanical and microstructural characteristics of the deposits formed under varied feedstock compositions.

The experimental data are further interpreted in view of a statistical model for deposition, considering the different deformation behaviour as well as the possibly even repulsive chemical interaction of the dissimilar particles. In this way, the model supplies a quantitative description of the observed deposition efficiency as a function of powder size and composition. The paper also discusses the scope of application of the findings and the model to other cold-sprayed composites or single alloy systems.

Keywords

Cold spraying

Composites

Bonding probability

Deposit microstructures

Deposit properties

Statistical model

1. Introduction

1.1 Cold Spraying and Bonding Mechanism

In the last two decades, cold spraying has been established as deposition process for metallic coatings and metal-ceramic composites [1, 2]. With a deposit thickness range of approximately 0.1 mm to some centimeters, the process is also suitable as additive manufacturing technique [3]. The principle of cold spraying is described in several textbooks [2, 4-6] and a variety of research articles [7-9]. The principles of determining particle acceleration and temperature as well as influences on critical conditions for bonding are included in a commercial software for forecasting deposit properties obtained by cold spraying [10].

Successful solid state powder deposition in cold spraying is enabled by supersonic velocities upon particle impact and associated high strain-rate deformation features at the contact interfaces [9, 11]. As already proposed in the early publications on the topic [4, 12], bonding only occurs if particles exceed a critical velocities v_{crit}, which is specific to the spray material. Plastic deformation and the formation of adiabatic shear instabilities and materials jets at contact interfaces are necessary prerequisites for bonding [1, 9, 13]. This knowledge of the basic mechanisms enabled correlations between process parameters and mechanical properties of the deposits, as well as targeted developments of cold spray techniques [11, 14]. When the critical velocity v_{crit} is just exceeded, only about 15 - 25% of the internal interface between particle and substrate are actually bonded [9]. If the impact velocity v_p is further increased, the bonding zone expands and improves the internal cohesion and associated properties of the resulting deposit. Based on numerical analysis, the ratio between v_p and v_{crit} at a given particle impact temperature can be defined as coating quality parameter [15].

$$\eta = \frac{v_p}{v_{crit}} \qquad (1)$$

The uniform description predicts properties and allows for an easy comparison between different parameter sets or powder sizes. Generally, high-quality coatings can be expected for conditions reaching $\eta > 1.5$ [13, 15].

1.2 Dissimilar Interfaces and Cold Spraying of Composites

The formation and local distribution of shear instabilities at contact interfaces depend decisively on the mechanical deformation behavior of the associated bonding partners. Ideally, impacting particle and subjected surface, i.e. the substrate material or the already deposited coating, show similar deformation, with the formation of a common interface and a common material jet [16]. If the mechanical properties differ, local shear rates of both materials at the interface get unbalanced and shear instabilities mainly only occur in the softer bonding partner [1, 2]. This can already be caused by temperature differences between particle and deposit surface [17]. Mostly, these dissimilarities in deformation behavior between deposit and substrate result in smaller adhesive strength as compared to cohesive strength in cold spraying. Thus, lowest bond strengths are obtained for rather rigid substrate materials [14]. Nevertheless, even for non-deformable substrates as for example alumina or other ceramics, conditions can be adjusted to allow metallic layer deposition by cold spraying [18-21]. In these cases, only the areas of shear instabilities within the metal particle ensure bonding. By faster deceleration and higher shear rates, volumes of shear instabilities in the particles are then even more concentrated and pronounced than for impacts onto a softer material, i.e. the kinetic energy is transformed into heat within a smaller volume, causing a steeper temperature gradient. However, for establishing common grain boundaries with the hard phase substrate two prerequisites must be meet: (i) Areas of shear instabilities must geometrically occur in the contact interface [2, 22], and (ii) the interface chemistry must allow for sufficient adhesion. These basic principles for dissimilar interfaces also apply for the cold spray deposition of composites.

Despite these challenges, cold gas spraying of composites is feasible and enables the combination of materials with different mechanical and thermal properties or special property combinations. Common approaches for processing a composite coating by cold spraying either use (i) a powder blend of the different spray materials, or alternatively, (ii) a pre-processed composite powder. Powder blends can be obtained by mixing before cold spraying, or by combining multiple powder feeders during the

spraying process, which then also opens the opportunity to produce graded coatings. In pre-processed composite powders, each powder particle already contains both components in the desired mixing ratio. Such composite powders can be produced by gas atomization, high-energy milling or agglomeration and sintering. While the first two methods produce dense particles, agglomeration-sintering provides an open, porous powder microstructure. Whereas the use of blends could suffer from individually different deposition efficiencies and difficult adjustment of composition, composite particles usually guarantee to meet the targeted volume fractions, however, involves additional efforts and costs in powder production. Compilations on the topic of cold gas sprayed composite coatings can be found, for example, in [2, 23-26].

The majority of studies deals with powder mixtures, since they are easy and flexible to produce. However, a deeper understanding about individual boundary condition for obtaining the desired compositions is still lacking. Thus, the present study tries to derive some general concepts that may be applicable to a wide variety of material combinations.

When spraying soft metal-metal mixtures such as Al-Zn, both components may be deposited in similar amounts [27]. However, for powder blends of materials with rather different thermo-mechanical properties and thus critical velocities, one common parameter set does not satisfy optimum impact conditions for both materials. Furthermore, dissimilar densities, thermal momentum and possible particle sizes as well as shapes effect acceleration and thus cause different impact conditions. Some optimization is possible via careful selection of the respective particle sizes, but may give rise to undesired geometrical relations in the deposit. In any case, the component with the higher critical velocity (for the selected particle size and temperature) will deposit with a lower deposition efficiency, as previously described in literature. Using for example Cu-Cr blends, only about half of the Cr present in the feedstock is incorporated into the coating during spraying [28]. Similar observations are made for Tribaloy T-700 in a softer matrix [29], or Ni-Ti composite coatings [30, 31]. For further examples see [32-34]. Counter measures deal with powder injection points to the spray jet, however require special modifications to the cold gas spray gun [35].

For low-pressure cold gas spraying (LP-CGS), metallic powders are almost always mixed with ceramic powders to achieve densification of the metal layers by the impact of the hard ceramic particles. In this process, the majority of the ceramic particles bounce off the surface again, as desired, or are merely loosely embedded in the metal matrix [36]. Commercially available are, for example, Al-Al_2O_3 or Cu-Al_2O_3 mixtures, which have also been extensively investigated [37-43] and [36, 44-48]. In addition, there are publications on experimental powder mixtures, for example with SiC or TiN reinforcement in an Al matrix [49-53]. The resulting coatings tend to retain higher volume fractions of ceramics as compared to Al-Al_2O_3 mixtures. Furthermore, since SiC or TiN is more strongly bonded to the Al matrix due to the more advantageous chemical interaction [24], the wear resistance of such sprayed coating is measurably improved.

Despite the problem that composite contents attained by cold spraying of powder blends are hardly predictable, so far no general model exists that allows for a desired forecast. A first approach to tackle the problem of describing impact probabilities, Klinkov et. al. set up a Monte-Carlo simulation for cold spraying of Al-Al_2O_3 powder mixtures [54] and validated this method against experimental work from Fernandez [55, 56]. The model assumes impacts of spherical particles on flat 2d surfaces. The probability of a successful particle deposition depends on the surface composition (area of Al compared to area of Al_2O_3) and bonding probability on this surface. The model fairly well describes the

experimental data for cold spraying of Al-A_2O_3, however it is not clear whether the specific assumptions would hold for more general approach.

1.3 Model system for a more general approach of cold spraying of powder blends

The present study combines a variety of analyses tools with model descriptions of dissimilar interfaces and generic bonding probabilities upon impact in cold spraying. In addition to own experimental input, the model is then also tested using literature data. Driven by possible technical applications in tuning thermal conductivity and thermal expansion between electronic components and heat sinks, tungsten-copper (W-Cu) and molybdenum-copper (Mo-Cu) composites serve as model systems for the present work.

However, dealing with refractory - Cu composites, additional influences have to be considered. Aside the very different melting temperatures and thus thermal softening behaviour, processing combination of W-Cu or Mo-Cu has to deal with highly different densities and materials strengths (or hardness). Moreover, due to their highly repulsive chemical interaction (heat of mixing > about +30 kJ/g-atom [57]), W-Cu or Mo-Cu alloys are immiscible even in the liquid state. Thus, for production of W-Cu composites, a prominently established process route uses infiltration of porous-sintered W components by liquid Cu. Semi-finished parts are available in different W contents of up to 90 vol-% (see supplements and [58]) to tailor their thermal expansion coefficient by the W content. Respective plates can be applied in electronics as thermal stress-reducing interlayers between electronic devices and underlying Cu or Al basis heat sinks.

To save costs for the production of such interlayers and tailor dimensions individually, alternative routes by using thermal spraying or cold spraying are of high interest. W-Cu composite coatings can be prepared by thermal spraying of powder mixtures or spray-dried powders. By using two separate powder feeders for blending fine W powder with Cu within the process, vacuum plasma spraying allows to transfer the refractory content almost completely into the sprayed coating [59, 60]. Similarly, with appropriately adapted particle injection into the plasma jet, atmospheric [61] or water-stabilized plasma spraying [62] can produce W-Cu coatings with W contents of up to 85 wt%. Applying cooler spraying processes such as high velocity oxy-fuel (HVOF) spraying, refractory composites coatings are also obtained. However, the W content in the coating (24 wt.%) is significantly lower than that of the original powder mixture (87 wt.%) [63].

Only a few articles have been published on cold spraying of W-Cu composite coatings. Using agglomerated-sintered W-Cu powders with W contents of 75 wt.% by spray drying and sintering procedures, cold spraying resulted in coatings containing about 40 wt.% of the refractory, even with such composite feedstock suffering from substantial hard phase losses [64]. Coating of W particles with Cu has been suggested as a promising alternative, but local separations are already evident in the interface between W and Cu in the starting powder [65]. The authors report that powders with 80 wt% W can be processed to coatings with about 57 wt% W. For the case of feedstock blends, different fine (average diameters $d_{Cu,fine}$ = 20 µm) and coarse ($d_{Cu,coarse}$ = 50 µm) Cu powders were mixed with fine W powder (d_W = 10 µm) and applied by cold spraying [66]. In the final deposits, about 60% and 50% of the originally present W were embedded by using the mixtures with fine and coarse Cu powder, respectively. In summary, according to the few literature data for cold spray deposition of W-Cu composites, not much more than about 50 % of the refractory originally present in the powder can

retained in the composite, irrespective of the type of powder production process. So far, there are no data published on cold spraying of Mo-Cu.

The few reports on combinations of W or Mo with Cu indicate influences by interface chemistry on bonding. Thus, the combination of methods and model descriptions given in the present study aims to shed more light into the role by interface chemistry into cold spray deposition of W- Cu and Mo – Cu composites.

2. Materials and Methods

2.1 Materials

For processing the different composites by cold spraying, blends of gas atomized Cu and sintered and crushed refractory metals were prepared. The use of similar or different sizes, here termed fine and coarse, in the respective mixtures of Cu with W or Mo powder was aimed to study possible sizes effects on deposit microstructures. Details on the powder are supplied in Table 1 and Figure 1. Thus, the different powder blends contained refractory metal particles in (i) similar sizes to the Cu particles, as well as (ii) in sizes that were significantly finer or (iii) significantly coarser.

Name	**Production method**	**Size distribution**	**Producer**
Cu_{fine}	Gas atomized	-22 + 5 µm	TLS Technik GmbH & Co Spezialpulver KG, Germany
Cu_{coarse}	Gas atomized	-38 + 16 µm	TLS Technik GmbH & Co Spezialpulver KG, Germany
W_{fine}	sintered	-15 + 5 µm	H.C. Starck, Germany
W_{coarse}	sintered	-45 + 22.5 µm	H.C. Starck, Germany
Mo_{fine}	Sintered and crushed	-22 + 5 µm	H.C. Starck, Germany
Mo_{coarse}	Sintered and crushed	-45 + 15 µm	H.C. Starck, Germany

Table 1: Used powders for spraying of composite coatings

The Cu powder particles have a spherical shape, as typical for a production route by inert gas atomization of the melt. In contrast, the shape of refractory metal powders is angular and blocky by milling from originally sintered bodies.

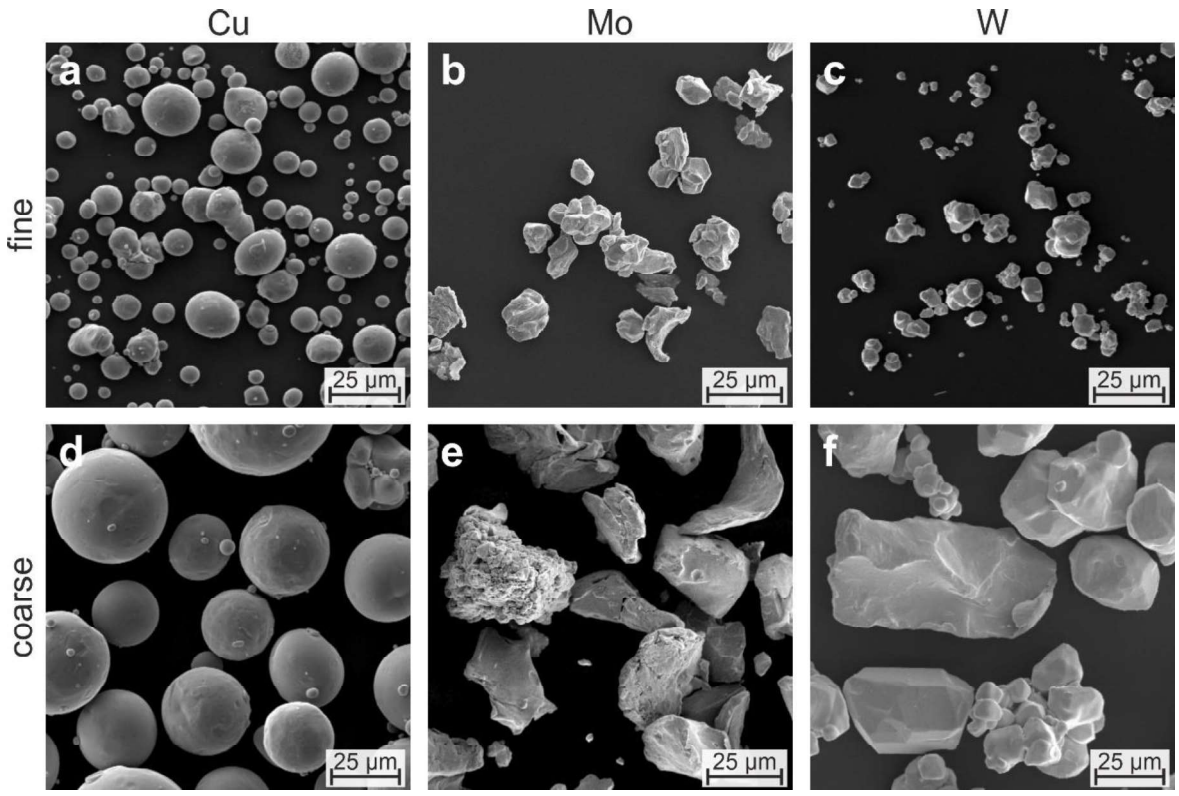

Figure 1: Morphologies of the different feedstock powders used for processing the composite coatings. Cu, Mo, W each in coarse and fine particle sizes. The gas atomized Cu powders have a uniformly spherical morphology, while the sintered-crushed Mo and W particles have an angular and irregular shape.

The powders were weighed and mechanically mixed in a defined ratio, and then fed to the spraying process by a single powder feeder. The weight ratios were adjusted to contain refractory metal volume contents in a range from 30% to 70% in the powder mixture.

As substrates, pure copper (Cu) and aluminum alloy (AlMg3) plates were used. Copper and aluminum are taken here as substrate materials due to possible applications as heat sinks in power electronics.

2.2 Cold spraying

The different powder blends were sprayed by using the HSU prototype for the Kinetics 8000x cold spray system from CGT, Ampfing, Germany, and nitrogen as process gas. The process gas pressure was set to 40 bar. By using nozzle type D24 WC-Co (CGT, Ampfing, Germany), the spray parameters were systemically varied by using different process gas temperatures for selected powder mixtures, as listed in Table 2.

RM-powder	**Cu powder**	**vol.-% RM**	**vol.-% Cu**	**T_{gas} [°C]**
W_{fine}	Cu_{coarse}	50	50	700 / 800 / **900**
W_{coarse}	Cu_{coarse}	30	70	900

W_{coarse}	Cu_{coarse}	50	50	700 / 800 / **900**
W_{coarse}	Cu_{coarse}	60	40	900
W_{coarse}	Cu_{coarse}	70	30	900
W_{coarse}	Cu_{fine}	50	50	600
Mo_{fine}	Cu_{fine}	30	70	600
Mo_{fine}	Cu_{fine}	50	50	500 / **600** / 700 / 800
Mo_{fine}	Cu_{fine}	60	40	600
Mo_{fine}	Cu_{fine}	70	30	600
Mo_{coarse}	Cu_{fine}	50	50	600

Table 2: Mixing ratios and spray parameters for the composite coatings. p_{Gas} = 40 bar, process gas N_2, nozzle D24 WC-Co, spray distance 60 mm.

Selected samples were heat treated after spraying to test whether this could strengthen the layer cohesion. The heat treatment took place under ambient air atmosphere for one hour at different temperatures (400 / 600 / 800°C).

2.3 Window of deposition / calculation of impact conditions

The impact conditions of the spray particles, i.e. the impact temperature and velocity, were estimated using a one-dimensional, stationary and isentropic calculation. The fundamentals of this calculation were developed in the work of Stoltenhoff [8] and Schmidt [13, 67]. For the present study, the commercially available KSS software was used (KSS Kinetik Spray Solutions GmbH, Buchholz, Germany) [10].

The software calculates velocities and temperatures of process gas and powder particles over the axial path from powder inlet in the pre-chamber, through the nozzle and the free jet down to the bowshock directly in front of the substrate. Input parameters are nozzle geometry, material data for gas and powder, as well as spray parameter sets (process gas pressure, temperature, etc.). Output parameters concern the impact conditions of the particles, e.g. their velocity and temperature at the point of first contact with the substrate surface. In this isentropic approach, effects by boundary layer friction, the heat exchange with the nozzle wall as well as possibly occurring compression shocks within the gas flow are considered by correction functions, as obtained by tuning to 3D fluid mechanical simulations for providing reliable values concerning particle impact conditions [67]. The particle impact conditions are superimposed with calculated, temperature dependent critical velocities [1]. In order to relate the

impact conditions to the critical impact conditions and thus to obtain information on the achievable properties, the deposit quality parameter η introduced by Assadi [15] is used.

2.4 Optical microscopy / SEM and determination of volume fractions

Cross-sections of the sprayed coatings were metallographically prepared as follows: Specimens were embedded in suitable resins (Bakelite-based hot embedding agent PolyFast with carbon fibers for scanning electron microscopy and cold-curing, 2-component epoxy resins EpoFix from Struers for optical microscopy) and grinded in subsequent steps. For polishing, diamond suspensions with grain sizes from 9 µm to 1 µm with a water-based lubricant were used. An oxide polishing suspension (OP-S or OP-U) with a grit size of 0.25 µm was used as the final polishing step. Automatic grinding and polishing machines and the appropriate consumables from Struers, Germany, were used.

Coating microstructure and the bonding to the substrate were investigated using an optical microscope of type DM 4000M (Leica, Germany). The contents of pores or refractory metal components within the deposits were quantitatively evaluated by image analysis software (KS 300 3.0, Zeiss, Germany).

Selected cross-sections and impact morphologies of individual particles were investigated by scanning electron microscopy (SEM Quanta 650 from FEI, Netherlands, as well as LEO 1550 Gemini FE-SEM with SmartSEM software from Zeiss, Germany). Typically, an acceleration voltage of 20 kV and a working distance of about 10 mm were employed.

2.5 Mechanical tests

The tubular coating tensile test (TCT) described in DIN 32535 and in [68] was used to analyze the cohesive strength of the composite coatings. In this test, two cylindrical specimens with a diameter of 25 mm are bolted face to face for depositing a coating on the common mandrel of this sample. The unbolted sample is then used for tensile testing. For the evaluation of the ultimate tensile strength (UTS), the applied force at fracture is related to the area of the coating cross-section. For calculating the UTS, the determined TCT-strength must be multiplied by a notch factor of 1.5 [68]. The tests were carried out with a tensile testing machine from Zwick / Roell (Germany).

2.6 Electrical conductivity

For cold sprayed coatings, analyses of electrical conductivity so far proved as suitable tool for assessing the deposit integrity. The electrical conductivities were determined by means of eddy current measurements at sample surfaces in accordance with ASTM E1004 (Sigmascope SMP 10-HF with sensor ES40HF, Fischer, Germany). The applied frequency of 1250 kHz should guarantee that the skin depth (60 µm for Cu, manufacturer's specification) is significantly lower than the coating thickness (at least 200 µm). Before the measurement, the sample surfaces were ground to minimum 6 µm finish to avoid influences by the coating roughness.

2.7 Electrical conductivity models for composites

The electrical conductivity can be used as measure for bonded internal interfaces. In cases of composites, this allows to distinguish bonding types, means whether the second phase particles are bonded by material to material connection or just mechanically clamped within the matrix. For the respective distinction, the measured conductivities were compared to different models for electrical conductivities in composite materials taken from literature.

If the different phases in the composite are layered perpendicular to the current direction, this corresponds to an electrical series circuit, in which the total resistance is given by the sum of the individual resistances [69, 70]. With volume fractions A_W and A_{Cu} and resistivities ρ_W and ρ_{Cu} of W and Cu, respectively, the resistivity of a W-Cu composite $\rho_{comp,\ series}$ can be expressed as:

$$\rho_{comp,\ series} = A_W \cdot \rho_W + A_{Cu} \cdot \rho_{Cu} \qquad (2)$$

After replacing the specific resistance by the specific electrical conductivity ($\sigma_{el,\ W} = \frac{1}{\rho_W}$) and suitable transformation, the conductivity of the composite coating is given by:

$$\sigma_{el,\ Komp,\ serie} = \frac{\sigma_{el,\ W} \cdot \sigma_{el,\ Cu}}{A_W \cdot \sigma_{el,\ Cu} + A_{Cu} \cdot \sigma_{el,\ W}} \qquad (3)$$

This model partially describes the actual geometric arrangement in the composite coating, although one of the phases - the refractory metal - is not continuously present as a single layer.

If the two phases are arranged parallel to the current direction, total electrical conductivity should be described by an electrical parallel circuit model [70]. Such models are also applied to cases of phase mixtures formed by solidification of immiscible systems [70-72]. As an example, Fuhrmann [71] interpreted the phase formation in the non-miscible W-Cu system by isolated W crystallites that initially crystallize in the melt and the solidification of Cu then forming the embedding matrix. Analyses of W-Cu rods produced in this way confirm that the electrical conductivity can be described by parallel circuit as the sum of the individual conductivities, weighted according to the volume fraction:

$$\sigma_{el,\ comp,\ parallel} = A_W \cdot \sigma_{el,\ W} + A_{Cu} \cdot \sigma_{el,\ Cu} \qquad (4)$$

The assumptions of this model might also describe the microstructure, i.e. the phase distributions of the cold gas sprayed composite coatings.

2.8 Model for impact statistics

In cold spraying of powder blends, individual η ratios give an estimate about coating quality, and ultimately, whether deposit formation is possible at all. However, for a comprehensive description of the probability that particles adhere to the surface consisting of different composite phases, suitable statistical models must be developed. These have to include potential direct interactions, as well as effects of geometric boundary conditions, the latter arising from different deformation behavior upon impact and from different particle size distributions in the blend.

As a first approach, a simple, two-dimensional numerical simulation model is developed to include the type of interaction and different particle sizes. The model describes the successive coating buildup with "soft" and "hard" particles onto already deposited material by the following basic assumptions:

An impacting particle will only stick if the hard phase coverage of the existing surface does not exceed a specific threshold. This implies a sufficiently high coverage with the softer component as a prerequisite for subsequent adhesion of following particles of both constituents. Furthermore, the model takes into account that binding of hard to softer material occurs only with a certain adhesion probability. This adhesion probability can be understood as the idealized deposition efficiency of an impinging hard particle on a soft substrate. The simulation takes four parameters into account, in detail the threshold values for the coverage $B_{soft\text{-}hard}$ and $B_{hard\text{-}hard}$ and the adhesion probabilities $H_{soft\text{-}soft}$ and $H_{hard\text{-}soft.}$ In this way, the model compiles effects of dissimilar interfaces with different bonding behaviors.

In the following, the structure, procedure and results of the model are illustrated using the example of a Cu (soft) – W (hard) powder mixture. Adhesion will be obtained as long as the non-bonding interface fraction, here corresponding to the W content in the surface/interface, does not exceed a certain threshold value. Respective threshold values depend on the type of impacting particle, here Cu or W.

A schematic of the model is given in Figure 2. The surface is assumed as a point lattice. Each point is assigned with properties of the material class (Cu or W). A 2000 × 2000 point grid was chosen to represent an area of 2 mm × 2 mm at a resolution of 1000 pixels per mm. Initially, the (substrate) surface consists entirely of Cu. The particles are represented as circular areas with diameters d_{Cu} and d_W. These diameters correspond to the mean diameter of the particle size fraction (D50) of the powders used in the experiments, see Table 3. In the present case, a Cu particle can only adhere if it encounters an – even small – fraction of Cu on the surface to which it can bond. In contrast, a W particle requires a large proportion of Cu on the surface, in which it can be embedded. If the described conditions are met, the particle will stick to the surface. In the simulation, the circular area will be completely covered with the respective material of the impacting particle. After that, the impact of the next particle is simulated, now taking the new configuration as point lattice to adhere to.

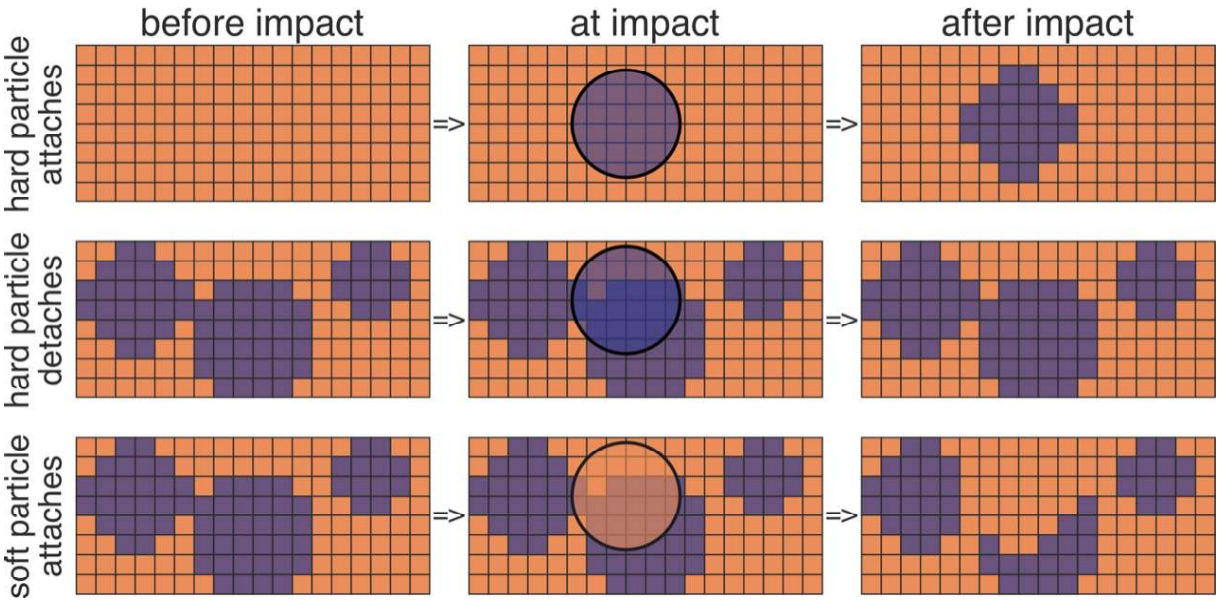

Figure 2: Schematic of the dissimilar impact scenarios for different time steps upon impact according to the model for the examples of W (blue) or Cu (orange) particles onto W-Cu surfaces. The particles adhere or detach depending on the W ratio being present in the surface and on the bonding probability to Cu.

Name	Particle size distribution	d (here D50) [µm]
Cu_{fine}	-22 + 5 µm	14
Cu_{coarse}	-38 + 16 µm	27
W_{fine}	-15 + 5 µm	10
W_{coarse}	-45 + 22,5 µm	34
Mo_{fine}	-22 + 5 µm	14

Table 3: Particle diameters used for the simulation

The deposition of particles at randomly selected positions on the surface is successively simulated in the sequence of single events. The particle fraction of Cu particles p_{Cu} and W particles $p_W=1-p_{Cu}$ are calculated from the volume fractions x_{Cu} and x_W, and particle volumes d_{Cu}^3 and d_W^3, respectively (examples in Table 4).

$$p_{Cu} = \frac{x_{Cu} \cdot d_W^3}{d_{Cu}^3 - d_{Cu}^3 \cdot x_{Cu} + x_{Cu} \cdot d_W^3} \qquad (5)$$

For each impact, it is tested whether the particle sticks or rebounds, depending on the W content in the surface to be covered by the impacting particle and the adhesion probability to the Cu. The different threshold values and adhesion probabilities have been determined by data fitting to the experimentally obtained deposit compositions for the powder mixture W_{coarse}-Cu_{coarse}. For an impacting W particle, no binding or adhesion occurs if the surface contains more than 5% W (B_{W-W} = 0.05). For an impacting Cu particle, binding occurs unless the surface contains not more than 90% W (B_{Cu-W} = 0.90). The probabilities of adhesion of Cu or W particles to Cu substrate were set to 100% ($H_{Cu-Cu} = H_{W-Cu} = 1$). So far, the physical interpretation of these simple model parameters has some limitations. However, they at least provide a good description of the geometric boundary conditions for bonding of dissimilar components with limited adhesion.

Powder mixture	d_W [µm]	d_{Cu} [µm]	x_W [vol.-%]	x_{Cu} [vol.-%]	p_W	p_{Cu}	Number of particles
W_{coarse}-Cu_{coarse} 50/50	34	27	50	50	0.33	0.67	23,000
W_{coarse}-Cu_{coarse} 30/70	34	27	30	70	0.18	0.82	29,000
W_{coarse}-Cu_{coarse} 70/30	34	27	70	30	0.54	0.46	16,000
W_{coarse}-Cu_{fine} 50/50	34	14	50	50	0.07	0.93	$1.2 \cdot 10^6$
W_{fine}-Cu_{coarse} 50/50	10	27	50	50	0.95	0.05	$3.0 \cdot 10^6$

W_{fine}-Cu_{fine} 50/50	10	14	50	50	0.73	0.27	$4.0 \cdot 10^6$

Table 4: Examples of input variables for the simulation

The total number of iterations depends on the number of particles used in the experiment: For the DE measurements, about 35 g of powder was sprayed onto an area of 50 × 65 mm². From the mass of the individual particles W and Cu (via d_W, d_{Cu} and the densities ρ_{Cu}, ρ_W) and their mixing ratio (converted to wt%), the number of particles in these experiments was determined and extrapolated down to the 2 × 2 mm² area used in the simulation. The particle number thus strongly depends on the particle size and varies between 10,000 and 4.3 million, examples of which are given in Table 4

As results, the simulation supplies data on the deposition efficiency (DE) for the powder mixture and for the individual portions of species (W or Cu) being embedded after the specified number of spray particles or iteration steps. The deposition efficiency of the individual components is calculated from the ratio of the number of sprayed particles $n_{sprayed}$ to the number of particles $n_{adhering}$ (the numbers also correspond to the weight and volume ratios, since the particle sizes of the different species are taken as fixed (D50) in one set of simulations). The relationship shown in equation (6) also applies analogously to Cu.

$$DE_W = \frac{n_{W,adhering}}{n_{W,sprayed}} \tag{6}$$

The deposition efficiency of the powder mixture takes into account the different particle masses and is therefore, as in the experiments, a ratio of coating mass to correspondingly fed powder mass:

$$DE_{powder\ mixture} = \frac{n_{Cu,adhering} \cdot \rho_{Cu} \cdot d_{Cu}^3 + n_{W,adhering} \cdot \rho_W \cdot d_W^3}{n_{Cu,sprayed} \cdot \rho_{Cu} \cdot d_{Cu}^3 + n_{W,sprayed} \cdot \rho_W \cdot d_W^3} \tag{7}$$

Initially, different threshold values for the W fraction in the surface, above which the particles would bounce off, were tested for the W_{coarse}-Cu_{coarse} powder mixtures until the simulation was able to reproduce the experimental data. The full procedure was then tuned to the full deposit volume and final parameter adjustment.

3. Results

3.1 Particle impact conditions and critical velocities for bonding

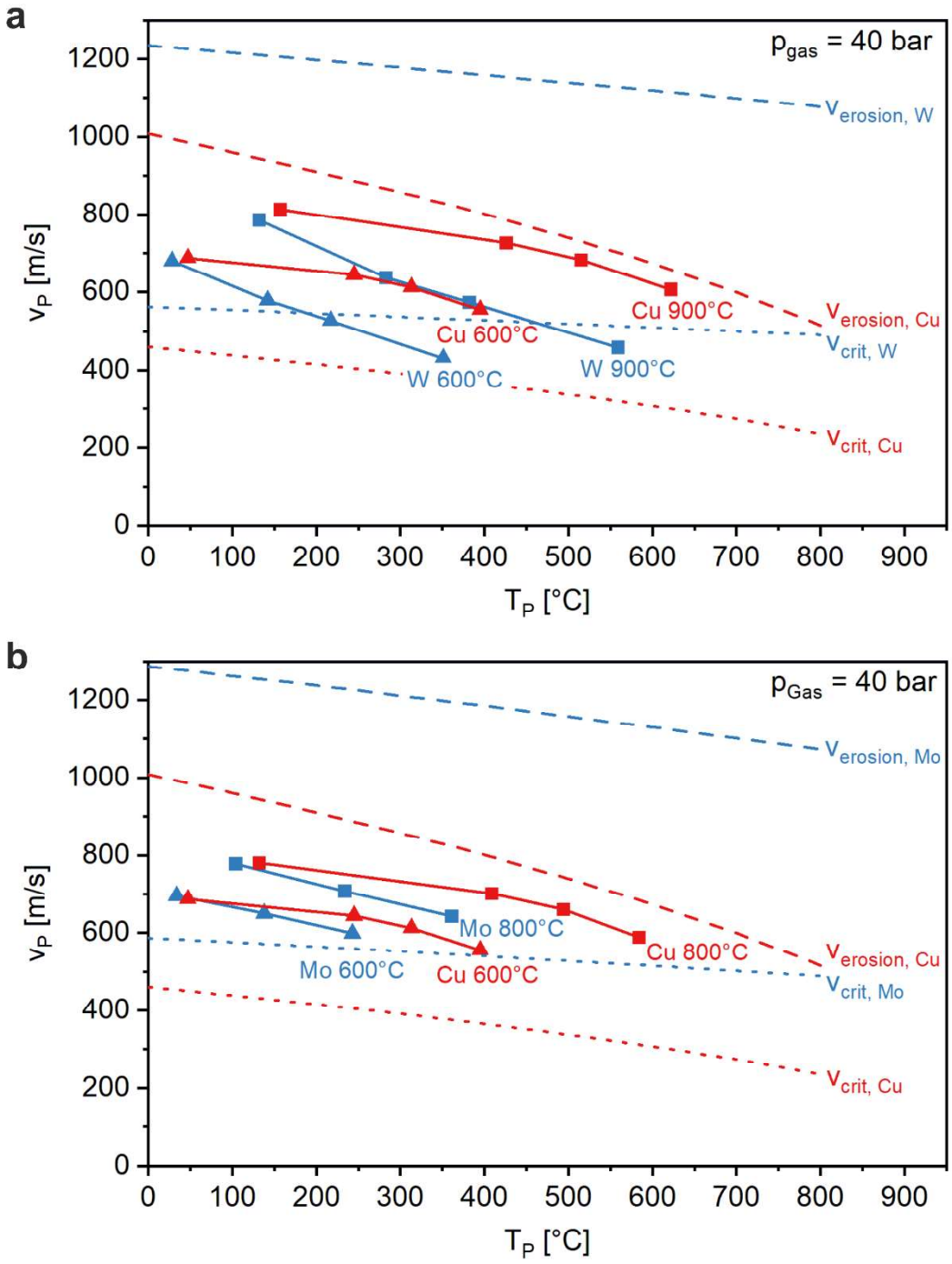

Figure 3 shows the individual impact conditions and critical velocities as windows of deposition for W / Cu (a) and Mo / Cu (b) blends. For the case of W / Cu, the particle impact conditions (v_P, T_P) were calculated for the fine and coarse powders that are used in the blends and for two different process gas temperatures, 600°C and 900°C, while keeping the process gas pressure fixed to p_{Gas} = 40 bar. At T_{Gas} = 600°C, the particle impact conditions of the Cu powder are found well above the critical velocity. In contrast, at this process gas temperature, only the smallest W particles < 15 µm can reach the critical velocity. At a risen process gas temperature of T_{Gas} = 900°C, the particle impact conditions of W are slightly higher, now also allowing slightly bigger particles to bond. At this temperature, the impact velocities of the Cu particles are further increased to regimes, where hydrodynamic effects might cause

already a decrease in deposition efficiency (erosion velocity). For the combination of Mo and Cu, impact conditions are considered for process gas temperatures of 600 and 800°C and a process pressure of 40 bar. The general situation is similar to that of the W and Cu combination, however, critical velocities of Mo are slightly higher. Thus, critical impact conditions are only exceeded for fine particles, and preferably at the higher process gas temperatures of 800°C. For practical use of both material combinations, it should be considered here that process gas temperatures above 600°C may already lead to nozzle clogging for fine Cu powder particles. Thus, at the given parameter ranges, required shear instabilities for building-up composites will occur predominantly in Cu, with only minor contributions of the respective refractory metal.

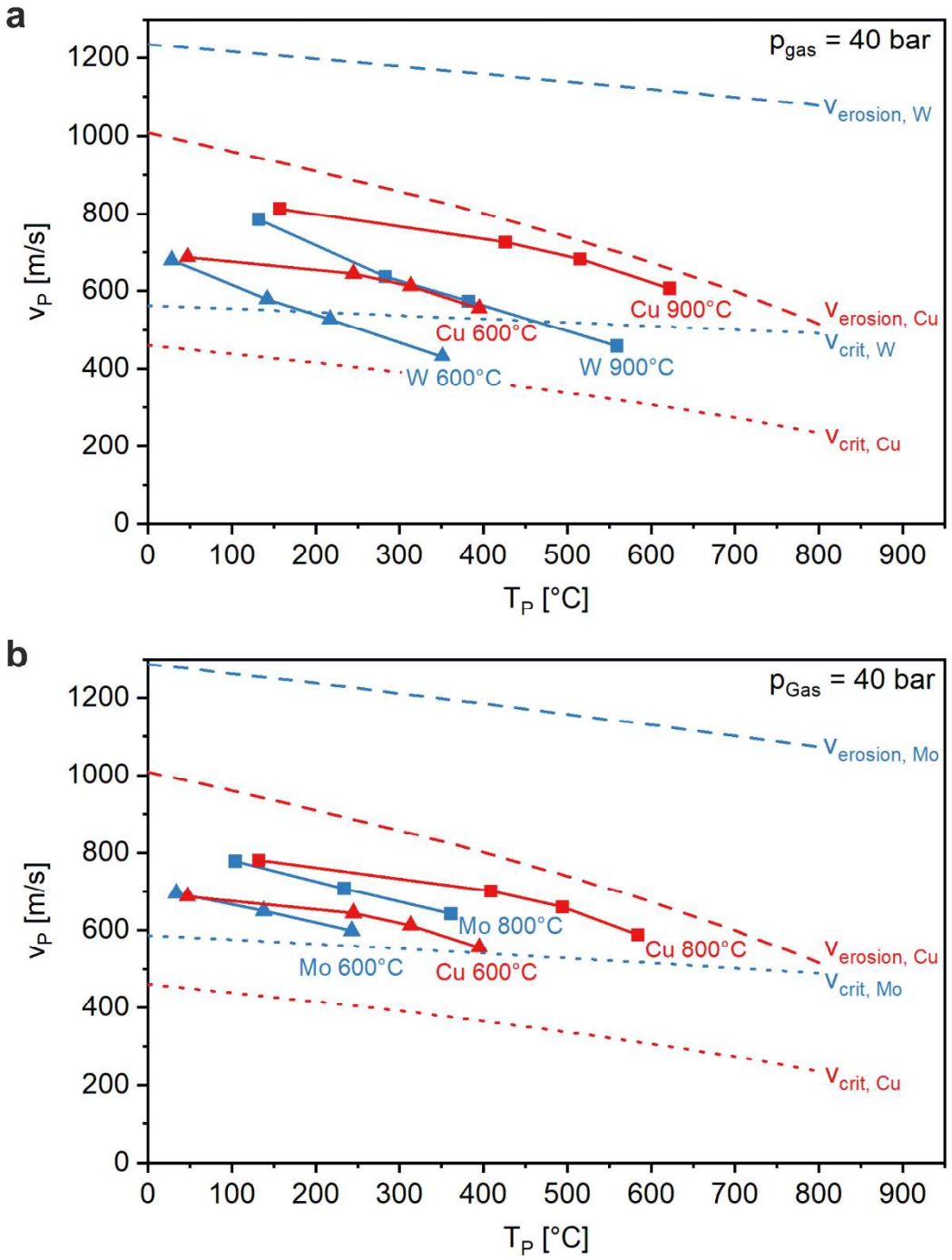

Figure 3: Impact conditions and windows of deposition, (a) for W-Cu powder mixtures at a process gas pressure of p_{Gas} = 40 bar and for two process gas temperatures T_{Gas} = 600; 900°C. Particle diameters

corresponding to the powder fractions: Cu_{fine} = -22+5 µm and Cu_{coarse} -38+16 µm. W_{fine} = -15+5 µm and W_{coarse} = -45+22.5 µm. The point sequence for one set of spray parameter corresponds to different particle sizes: 5 / 16 / 22 / 38 µm in case of Cu, and 5 / 15 / 22.5 / 45 µm in case of W, (b) for Mo-Cu powder mixtures for a process gas pressure of p_{Gas} = 40 bar and two process gas temperatures T_{Gas} = 600 ; 800°C. Particle diameters corresponding to the powder fractions: Cu_{fine} = -22+5 µm and Cu_{coarse} -38+16 µm. Mo_{fine} = -22+5 µm. The point sequence for one set of spray parameter corresponds to different particle sizes: 5 / 16 / 22 / 38 µm in case of Cu and 5 / 13.5 / 22 µm in case of Mo.

3.2 Coating microstructures

The different powder mixtures successfully build up composite coatings upon cold spraying. Typical microstructures of cross-sections are shown in Figure 4, consisting of isolated single W or Mo particles embedded within a Cu matrix. While the Cu particles appear strongly deformed, W or Mo particles remain in their original shape and do not show significant plastic deformation. Direct contact between W or Mo particles is rarely observed. If present, respective interfaces are accompanied by cracks. Some porosity is visible in the cross-sections of the coatings, in sizes corresponding to W or Mo particles. This can probably be attributed to pullouts of loosely bonded refractory particles during metallographic preparation.

However, there are distinct differences in microstructures related to feedstock sizes. For W-Cu coatings containing coarse W and Cu particles, the refractory metal is rather homogeneously distributed within the Cu matrix (Figure 4a, b, c, d). By using fine W and coarse Cu powder, the refractory particles only decorate the boundaries between coarse Cu particles (Figure 4e, f).

For Mo-Cu coatings sprayed with fine powders of both, the refractory distribution is homogeneous (Figure 4g, h). The respective composite shows less pores than that of the W_{coarse}-Cu_{coarse} combination. Also, the combination of coarse Mo and fine Cu (Mo_{coarse}-Cu_{fine}) results in a rather homogeneous composite coating (Figure 4i, j), with Mo particles being embedded within the Cu matrix. However, mean sizes of embedded Mo particle sizes are smaller than that of the feedstock powder. The reason may be that larger particles do not reach the required velocity for bonding to the deposit surface.

From the microstructural analyses, it can be concluded that a homogeneous phase distribution in the composite is only obtained, if the hard phase particle sizes are similar or larger than that of the soft Cu matrix. In addition, the use of smaller particle sizes seems to be beneficial for reducing deposit porosities.

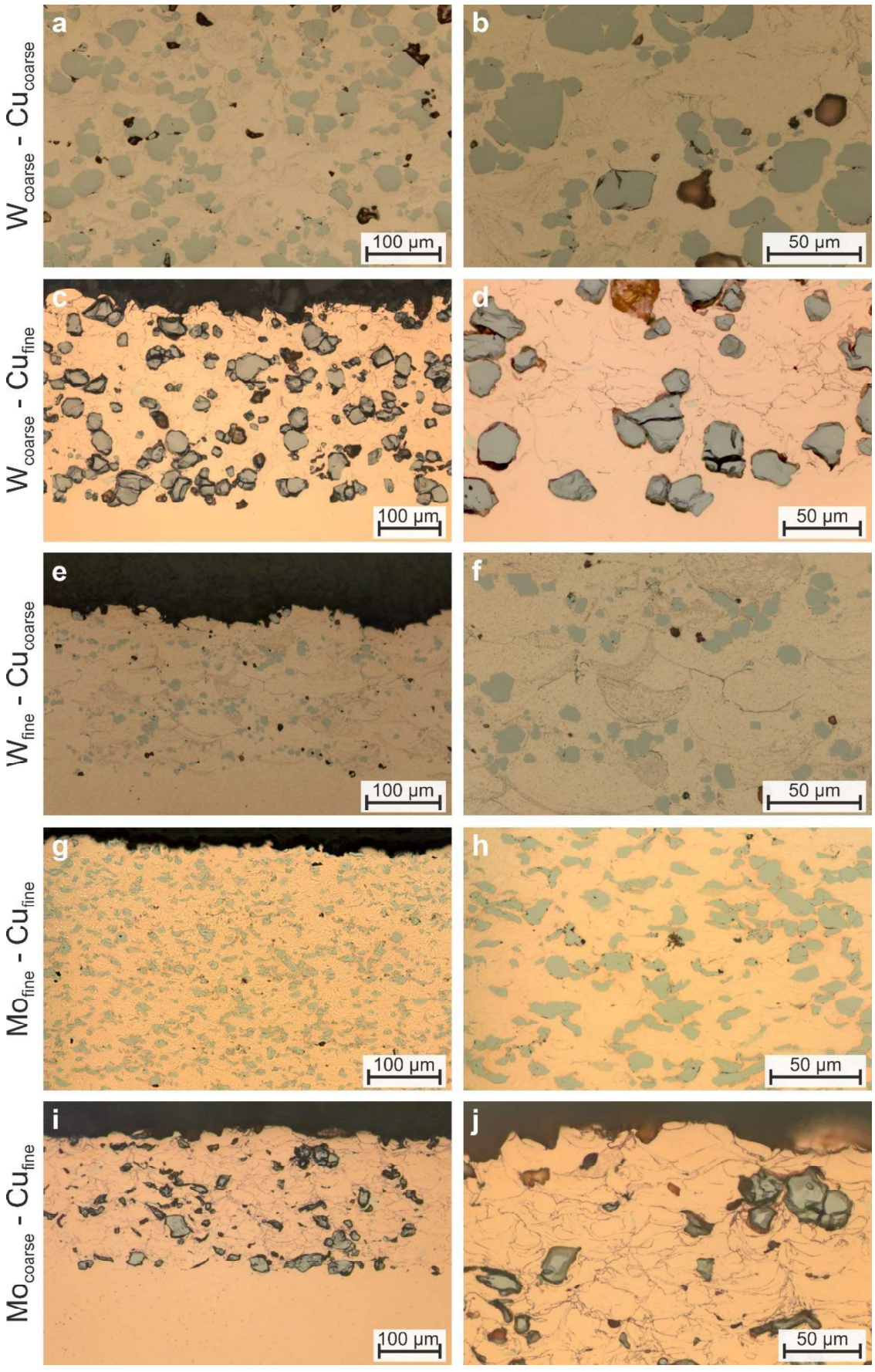

Figure 4: Microstructures of the cold gas sprayed composite coatings. (a, b) W_{coarse} - Cu_{coarse} with 36 vol.% W in coating (p_{gas} = 40 bar, T_{Gas} = 900°C). (c, d) W_{coarse} - Cu_{fine} with 20 vol.% W in coating (p_{gas} = 40 bar, T_{gas} = 600°C). (e, f) W_{fine} – Cu_{coarse} with 5 vol.% W in coating (p_{gas} = 40 bar, T_{gas} = 900°C). (g, h) Mo_{fine}

- Cu_{fine} with 22 vol.% Mo in coating (p_{gas} = 40 bar, T_{gas} = 800°C). (i, j) Mo_{coarse} - Cu_{fine} with 9 vol.% Mo in coating (p_{gas} = 40 bar, T_{gas} = 600°C). Isolated breakouts of particles during metallographic preparation are an indication of poor bonding within the coating.

3.3 Refractory volume fractions in W-Cu and Mo-Cu composite coating

The volume fractions of refractory metals within the composite coatings were derived by image analysis of the coating cross-sections. The respective results are summarized in Figure 5 in direct comparison to the refractory content present in the different powder mixtures. The displayed dashed lines represent deposit contents for powder blends of refractory metal particles with Cu particles of similar size at fixed parameter sets. Individual points indicate selected situations for using dissimilar sizes or other spray conditions. The example of the W_{coarse} - Cu_{coarse} mixture (blue line) corresponds to a process gas temperature of T_{Gas} = 900°C. The trends for the Mo_{fine} - Cu_{fine} blends (red line) are given for a comparatively low process gas temperature of T_{Gas} = 600°C. The grey dotted line indicates the ideal situation, in which all refractory metal particles from the powder mixture would be incorporated into the resulting coating, i.e. the fraction in the coating being identical to that of the original mixture.

The results in Figure 5 show that higher refractory contents in the powder blend result in an increased volume fraction in the deposit. However, the refractory contents in the deposit show an increasing deviation from nominal composition with rising amounts of refractory metal in the feedstock powder mixture. The higher the amount of refractory metal in the feedstock powder mixture, the more of that is lost during deposit build-up. It is expected that the curves run into a saturation limit for a maximum refractory metal content in the cold gas sprayed layer. For the given different process conditions (W-Cu: T_{Gas} = 900°C, Mo-Cu: T_{Gas} = 600°C), it can be estimated that these saturation limits are reached at less than about 40 vol. % of W, and less than about 20 vol. % of Mo within the deposit, respectively. Reaching overall lower refractory contents in cases of spraying Mo-Cu than for W-Cu blends can be attributed to the different critical conditions for bonding, and temperature limitations due to nozzle clogging, if using fine Cu-powder.

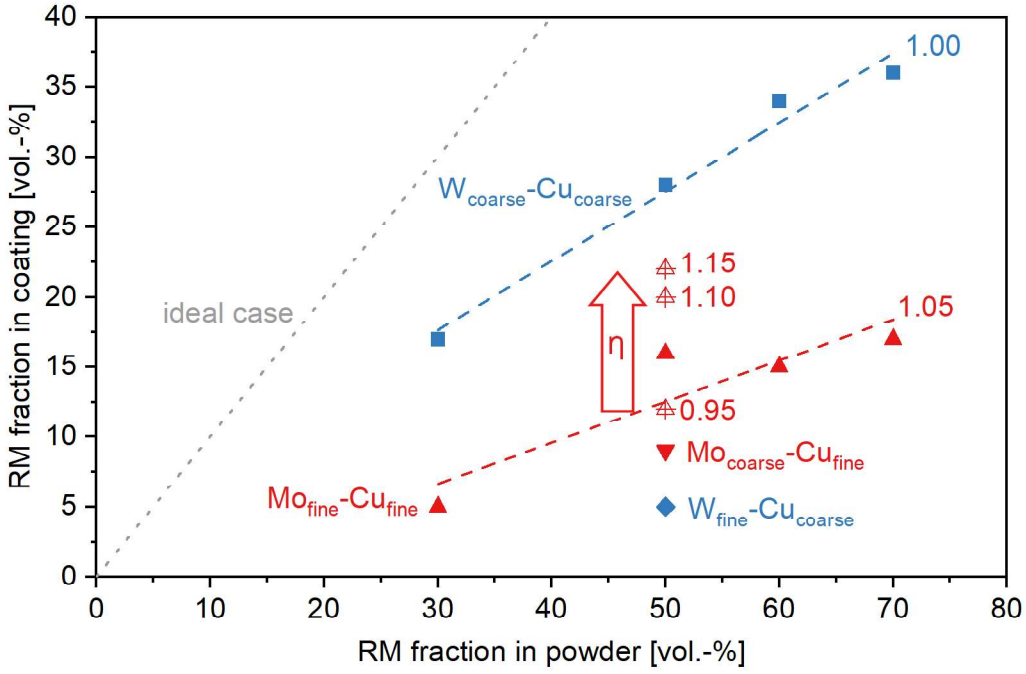

Figure 5: Refractory metal (RM) contents in the powder mixtures and in the cold gas sprayed coatings. Particle size combinations are given as inserts. In case of the composition with 50 vol. % Mo, the

influence by different spray parameters is indicated by the respective η-values for the impact of Mo. Increasing the process gas temperature and thus the η-value of the refractory metal leads to a higher hard phase content in the composite coating, shown here for the powder mixture 50 Mo_{fine} - 50 Cu_{fine} for η-values from 0.95 to 1.15 as indicated (red open triangles). The different blend compositions were sprayed at p_{Gas} = 40 bar and T_{Gas} = 900°C for W-Cu, and T_{Gas} = 600°C for Mo-Cu, respectively.

The comparison clearly shows that the refractory contents in the composites are highest for similar powder sizes of the feedstock constituents. Since small hard phase particles only decorate the interfaces between larger soft ones, only rather limited contents can be obtained. In the example of combining 50 vol. % of fine W with coarse Cu powder (W_{fine} - Cu_{coarse}, blue diamond symbol in Figure 5), the refractory content only reaches about 5 vol %, in contrast to 27 vol. % by using similar sizes of coarse particles in in the case of the W_{coarse} - Cu_{coarse} mixture. The situation is slightly different for using small soft and large hard particles. Using a mixture of 50 vol. % Mo in the the Mo_{coarse} – Cu_{fine} blend results in a refractory content of 9 vol. % in the deposit, in contrast to the 16 vol.% Mo being present after cold spraying the Mo_{fine} - Cu_{fine} coating. This difference could be due the fact that bonding probabilities of fine Cu impacting solely onto bigger Mo parts are lower as compared to those hitting a mixed Mo/Cu surface.

Increasing the process gas temperature and thus the η-values of both constituents of the blends leads to higher hard phase contents in the composite coating. Figure 5 includes examples for a refractory content of 50 vol. % in a Mo_{fine} - Cu_{fine} powder mixture and η-values for Mo ranging from 0.95 to 1.15, corresponding to an increase of the process gas temperature from 500°C to 800°C (red open triangles). Within this regime, the Mo content in the composite coating could be increased from 12 to 22 vol. %.

In summary it is advisable to select a similar powder size distribution for the two spray materials used (Cu and W or Mo) in order to achieve a higher hard phase content within the Cu matrix of cold sprayed composites (compare Figure 5 and Figure 11).

3.4 Tensile strengths of composite coatings

Figure 6 shows the tensile strengths of the different composite coatings, for convenience here being normalized to contributions by the Cu-matrix, i.e. for Cu-W:

$$TCT_{normalized} = \frac{TCT_{measured} \cdot 100}{100 - vol\%W} \qquad (8)$$

For the W_{coarse}-Cu_{coarse} composite coatings, the normalized strengths are nearly constant, regardless of the different refractory metal contents. This indicates that the applied load is mainly carried by the Cu matrix. Subsequent heat treatments (HT, open symbols) result in decreased composite strengths. This can be mainly attributed to recrystallization and respective softening of the Cu matrix. The strengths of the Mo_{fine}-Cu_{fine} composites are found within a similar range as those of the W-Cu deposits. However, for this combination, the normalized composite strengths show a slight increase with hard phase content. For this case, apart from the Cu-matrix, some of the dissimilar interfaces seem to support the overall composite behaviour.

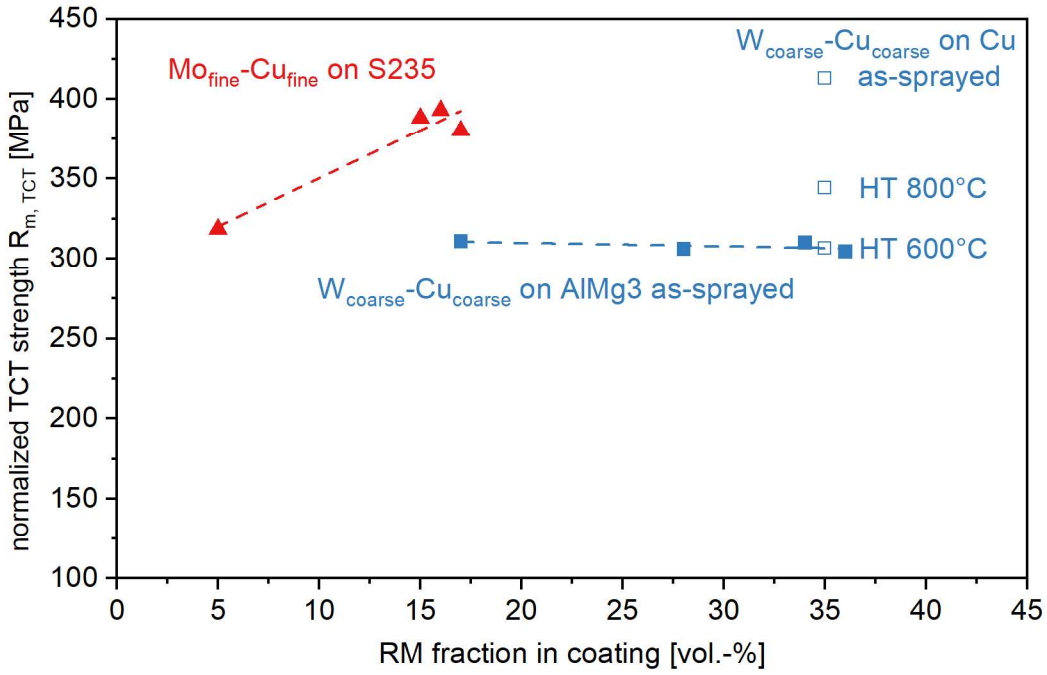

Figure 6: Tensile strengths of the different composite coatings, corrected for the refractory metal content. The different composites were produced at p_{Gas} = 40 bar and T_{Gas} = 900°C for W-Cu, and T_{Gas} = 600°C for Mo-Cu, respectively. The use of different substrates as well as deposit heat treatments is indicated by inserts.

After testing of the TCT specimens, the respective fracture surfaces were analysed by scanning electron microscopy. Examples of the facture topographies are given in Figure 7 and illustrate that any plastic deformation during testing solely occurs within the Cu matrix. In the as sprayed state (Figure 7a), typical pattern of work hardened material as well as also failure at non-bonded interfaces between Cu particles is observed. The W particles do not exhibit any plastic deformation and appear rather loosely bonded or embedded within the Cu matrix, as indicated by the gaps at the W-Cu interfaces. By the heat-treatment (Figure 7b), the Cu matrix got more ductile. Respective fracture surfaces of the matrix show dimple pattern, typical for plastic deformation. However, the heat treatment did not improve the situation for the W-Cu interfaces. As compared to the as sprayed condition, the gaps between at W-Cu got wider, possibly due to the larger local strain under the deformation of the soft Cu matrix.

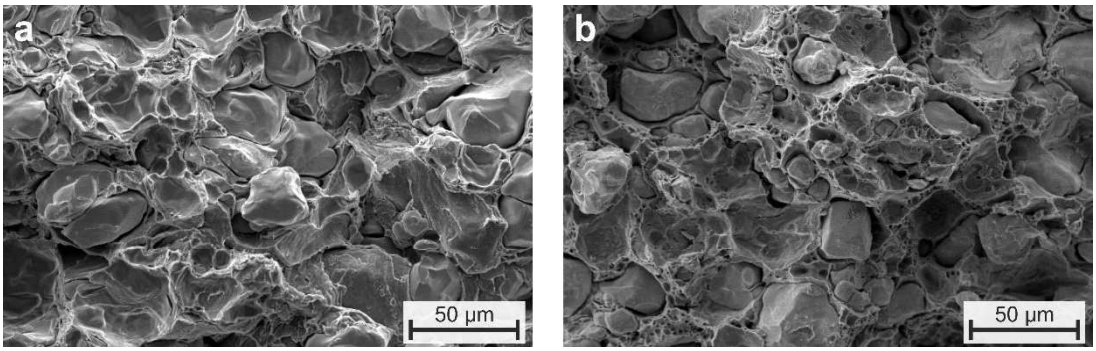

Figure 7: Fracture surfaces of W_{coarse}-Cu_{coarse} coatings in (a) as sprayed and (b) annealed condition after a heat treatment at 800°C for 1 hr. The deposit was produced with p_{Gas} = 40 bar and T_{Gas} = 900°C.

3.5 Electrical conductivities and appropriate circuit models for composites

From the microstructural analyses and the tensile test results, it is not clear yet whether the hard phase (W, Mo) particles are in direct metallurgical (conductive) interface contact or just in form-fitting loose contact with the surrounding Cu matrix in the as sprayed state. Detectable cracks with noticeable gap widths in fracture surfaces are probably widened during the testing procedure, i.e. are not obvious in the as sprayed condition. The results for the electrical conductivities should provide information on the existence of cracks at the W-Cu and Mo-Cu interfaces after initial deposit buildup.

Figure 8 compares the electrical conductivities of the cold gas sprayed composite coatings with data on composites prepared via liquid phase infiltration (porous sintered refractory metal samples infiltrated with liquid Cu) (data source see Table 6 in supplements [58]). For as deposited cold composites, the electrical conductivities show a nearly linear decrease towards zero with increasing refractory contents. In contrast, the infiltrated composites at high refractory content with some scatter strive towards the conductivity of the hard phases. The solid curves represent the electrical conductivities according to different models for composite materials and respective fitting to the experimental data. These models mainly differ with respect to the geometrical arrangement of the two phases in the composite and the reference states for pure hard phases.

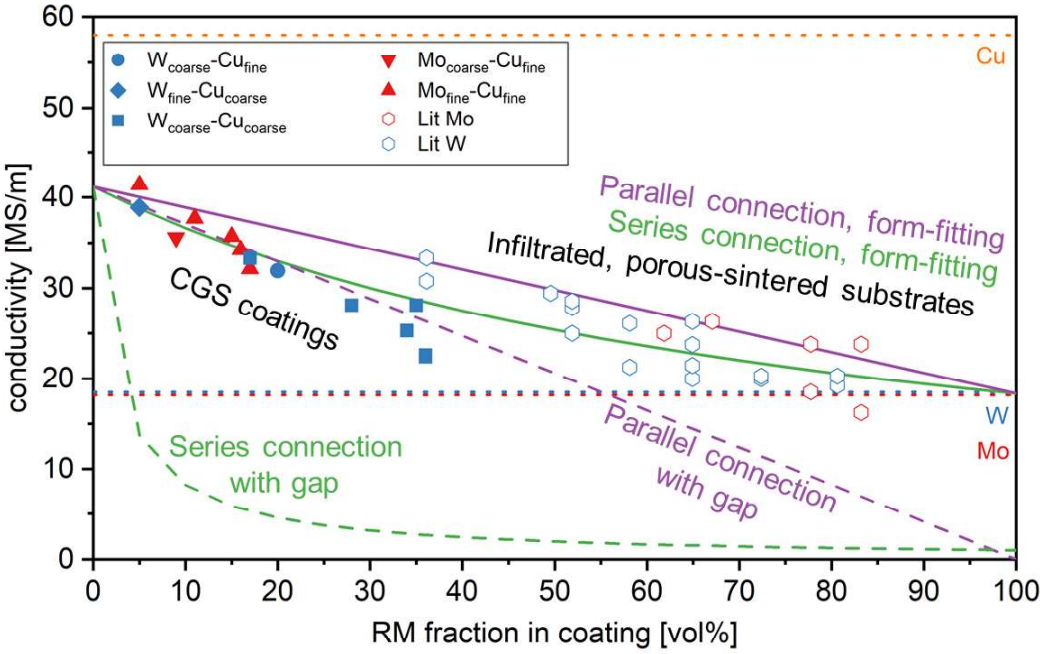

Figure 8: Measured electrical conductivities of the different cold sprayed composites in comparison to literature values (see Table 6 in supplements [58]) of Cu-infiltrated, porous-sintered W and Mo samples. The colored curves correspond to the model of series connection with W or Mo (green solid line) and non-conducting gaps / pores (green dashed line), and the model of parallel connection with W or Mo (purple solid line) and non-conducting gaps / pores (purple dashed line). The conductivity of the Cu matrix was set to 71% IACS, corresponding to 41.2 MS/m, to fit the models to the real measured conductivities. The cold spray coatings were processed at p_{gas} = 40 bar, T_{Gas} = 900°C and 600°C for W-Cu, Mo-Cu, respectively.

Using the conductivities of the different constituents as reference, the two models assume that the W particles are at least form-fitting bound into the Cu matrix. However, if the refractory metal - Cu interfaces are separated by gaps, electron transfer, i.e. current flow across the interface, would be interrupted. In this case, the overall conductivity of the composite coating would depend only on the

conductivity of the Cu matrix. The contribution of the non-bounded refractory particles would then have an effect similar to that of increased porosity in the matrix lowering the total conductivity (composite with insulating phase). For this case, the conductivity of the W particles (as well as of Mo particles) was set close to zero (dashed curves in Figure 8). In the parallel circuit model, the electrical conductivity of the composite coating then simply decreases linearly with increasing refractory metal content (violet dashed curve). In contrast, the series circuit model suggests a drastic drop in conductivity already at low W contents (green dashed curve).

The comparison of the different approaches in Figure 8 shows that the model of the series circuit with form-fitting contact (green solid curve) can adequately describe the conductivity data of the porous-sintered and Cu-infiltrated refractory metal composites given in literature (see Table 6 in supplements [58]). Here, W and Cu are each present as continuous, cross-linked phases that are connected by direct form-fitting contact. The framework of interconnected W particles and the plasticity of Cu ensure that shrinkage during solidification of the Cu melt and during cooling to room temperature does not lead to large-scale separations. In contrast, the conductivities of the cold gas sprayed composite coatings are best described approximately by the parallel circuit model assuming a gap at the W-Cu interface (purple dashed curve). This means that most of the interfaces between the refractory particles and the surrounding Cu-matrix get separated already during cold spraying or the respective cooling to room temperature afterwards, all together indicating no or at maximum weak dissimilar bonds. For cold sprayed Mo-Cu composites, the conductivities also seem to follow the description by the parallel circuit model with interface gaps. Within the covered regime with low hard phase contents, the data could also be described by serial circuits, but such would be in contrast to observed microstructures with isolated Mo embedded by a Cu matrix.

3.6 Statistical description for cold spraying of Cu-refractory composites

The analyses of cold sprayed W-Cu and Mo-Cu composite coatings with respect to microstructures and mechanical strengths show the following main results:

1) The deposited composites contain lower amounts of W or Mo as hard phase than the respective in feedstock powder mixture

2) W or Mo are enclosed as hard phases within a Cu-matrix. If existing, W-W or Mo-Mo interfaces not or only weakly contribute to bonding and composite strength

3) Internal interfaces between W or Mo and Cu are to high extent separated by gaps

In the following, these main findings are validated by a numerical impact model of soft / hard particles to describe the statistical probability of Cu-Cu, W-W and W-Cu (or Mo-Mo and Mo-Cu) interactions and resulting volume fractions of hard phases during composite coating build-up.

Figure 9 summarizes the results on experimentally determined and modelled deposition efficiencies of the W_{coarse} - Cu_{coarse} powder blends and the derived deposition efficiencies of the pure W and Cu components, respectively (T_{gas} = 900°C, p_{gas} = 40 bar). For this purpose, the measured volume fractions (compare Figure 5) were converted into weight fractions. The experimental results can be well described by the statistical model as given by the respective solid lines, reflecting the trends in overall as well as individual deposition efficiencies. For the uniform description of the deposition efficiencies by bonding probabilities, subsequent fitting procedures were applied. The best description by the

model is obtained with interaction parameters of $B_{W\text{-}W}$ = 0.05, $B_{Cu\text{-}W}$ = 0.90, $H_{W\text{-}Cu}$ = 1.00, $H_{Cu\text{-}Cu}$ = 1.00. $B_{W\text{-}W}$ reflects the very low probability of W particles to bond to W being present in the surface. In contrast, the probabilities of dissimilar bonds (W-Cu or Cu-W) are rather high.

At the given spray parameter set used here, Cu is deposited with efficiencies close to 100%. This high deposition efficiency of Cu is even maintained at rather high W contents in the powder blend. This indicates that even small amounts of Cu in the surface ensure bonding of impinging Cu particles. However, the deposition efficiency of the complete composite decreases significantly with increasing refractory metal content. This is because less and less amounts of refractory metal can be incorporated into the coating. At a rather low W content of 30 vol. % in the powder blend, the total deposition efficiency of the mixture is still comparatively high at 80%. However, only about 50% of the W from the starting powder is incorporated into the coating. At a high W content of 70 vol. % in the powder mixture, the overall deposition efficiency drops to about 40%, mainly by the low amounts of W, in detail only about 30% of the W originally present, being embedded in the coating. This can be explained by the increased probability of W impacting on W, which not or only to minor extent results in bonding.

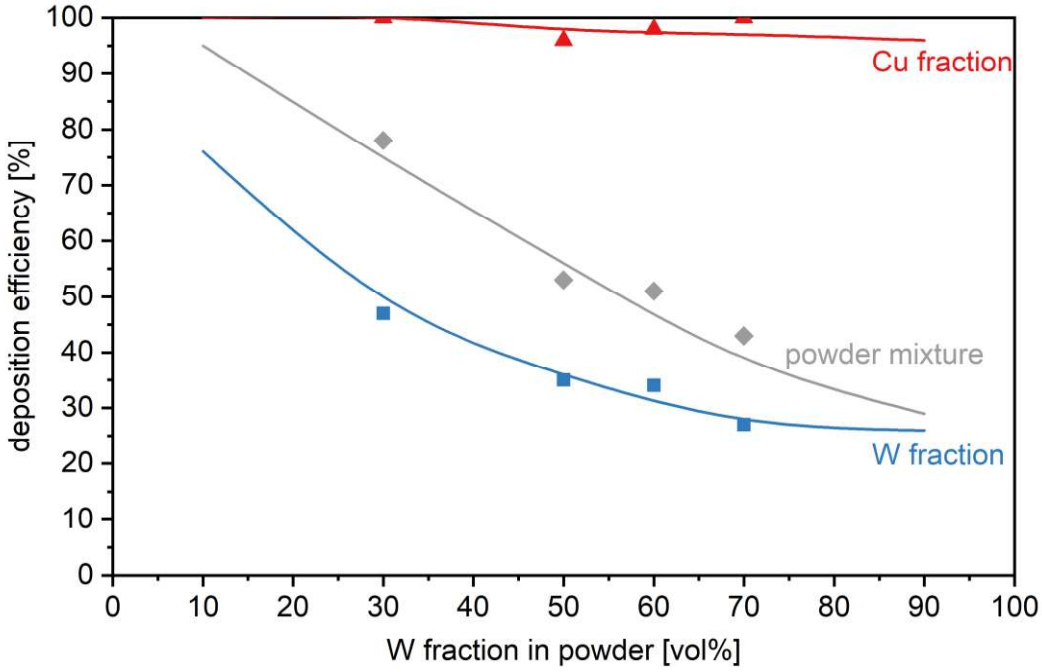

Figure 9: Deposition efficiencies of the W_{coarse}-Cu_{coarse} powder mixture for different volume contents of W within the feedstock. The deposition efficiencies are given for the overall mixture and for the individual amounts of W or Cu in the composites. The individual data points correspond to the experimentally determined values (as determined for p_{Gas} = 40 bar, T_{Gas} = 900°C). The curves represent the results of the numerical model. The parameters for the simulation of the bonding probability were determined to $B_{W\text{-}W}$ = 0.05, $B_{Cu\text{-}W}$ = 0.90, $H_{W\text{-}Cu}$ = 1.00, $H_{Cu\text{-}Cu}$ = 1.00.

A comparable trend is observed for Mo-Cu powder mixtures. Figure 10 shows the experimental deposition efficiencies for cold spraying of Mo_{fine} - Cu_{fine} powder blends (p_{Gas} = 40 bar, T_{Gas} = 900°C) during processing of Mo-Cu composites as global as well as individual deposition efficiencies (different symbols) as well as respective results from modelling (solid curves). The general trend of a decreasing deposition efficiency with increasing refractory contents in the powder blend is similar to that observed for W–Cu. As compared to W-Cu, however, the individual deposition efficiency of Mo is significantly smaller. At low Mo content of 30 vol. % within the feedstock, only less than 15 % of that

is embedded into the composite. The deposition efficiency of Mo slightly decreases with higher refractory contents in the blend. With higher refractory contents in the starting powder, the low amounts of bonded Mo leads to significantly reduced deposition efficiencies of obtained composites. The deposition efficiency of Cu is close to 100 % for all of the different compositions.

The low amount of embedded Mo in the composite bonding is reflected by the bonding probabilities in the simulation. Respective parameters were determined to $B_{Mo\text{-}Mo} = 0.15$, $B_{Cu\text{-}Mo} = 0.90$, $H_{Mo\text{-}Cu} = 0.15$, $H_{Cu\text{-}Cu} = 1.00$. The major difference to the W-Cu system concerns the bonding probability of Mo to Cu, with 0.15 instead 1 for the case of W-Cu. This means that the impacts of Mo onto Cu is much less likely to result in particle adhesion than those of W. Possible reasons might given in different spray parameter sets with a process gas temperature of 600°C in case of Mo-Cu instead of 900°C used for W-Cu or the different particle sizes (Mo-Cu: fine, W-Cu: coarse).

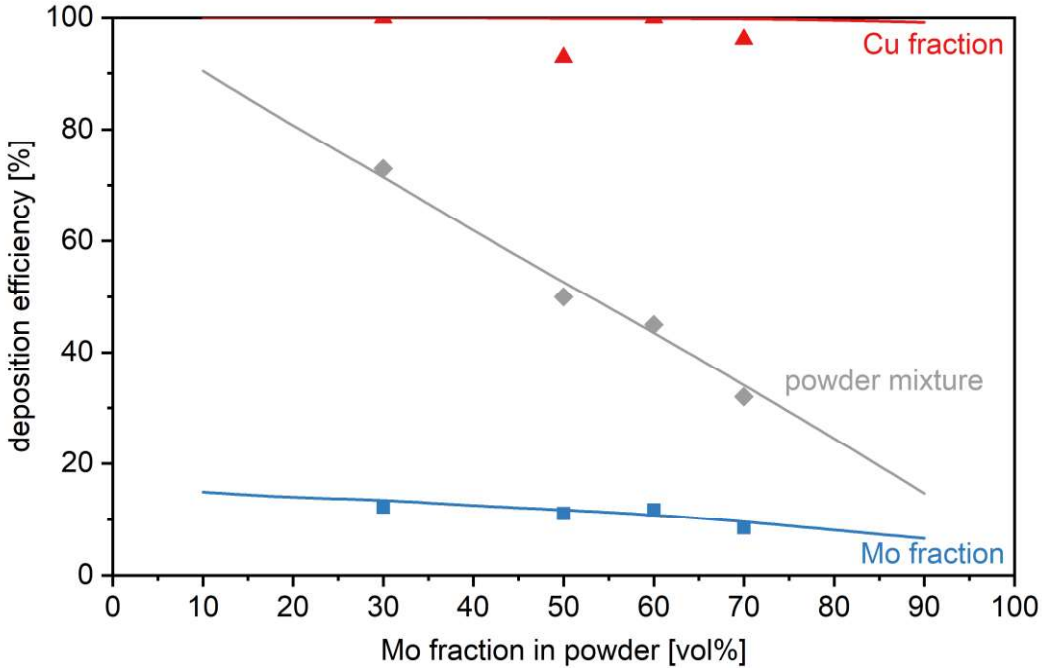

Figure 10: Comparison of experimentally determined (symbols) and simulated (solid lines) deposition efficiencies for powder mixtures Mo_{fine} - Cu_{fine} during composite build-up by cold spraying ($p_{gas} = 40$ bar, $T_{Gas} = 600$°C). Throughout, only about 10 % of the Mo present in the mixtures is incorporated into the coating. Simulation parameters were adapted to $B_{Mo\text{-}Mo} = 0.15$, $B_{Cu\text{-}Mo} = 0.90$, $H_{Mo\text{-}Cu} = 0.15$, $H_{Cu\text{-}Cu} = 1.00$.

4. Discussion

4.1 Microstructural development

The critical velocities required for bonding and respective windows of deposition for W or Mo on the one hand and for Cu on the other hand (compare

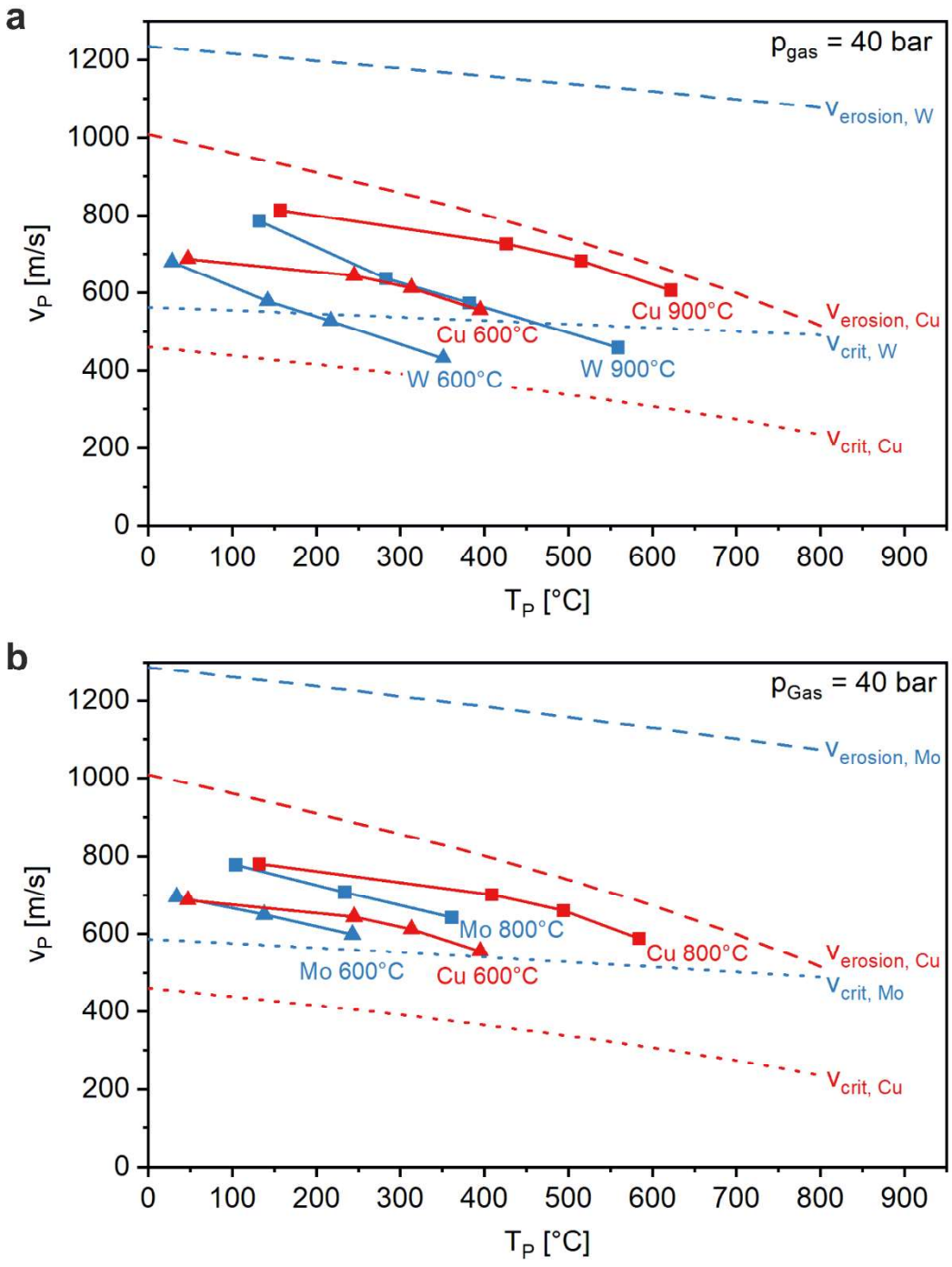

Figure 3) differ significantly and show only a very limited overlap. Consequently, according to the calculated impact conditions for the different powders, different extents of particle deformation are expected, and indeed have been observed in cross section microstructure analyses (compare Figure 4). Cu particles are highly deformed and are obviously well bonded to each other. In contrast, W or Mo show almost no deformation, and direct contact between these refractory metal particles is rather rare: if at all observed, the interfaces appear loosely bonded, even though their impact velocity exceeds the critical velocity, which should in principle allow for bonding. Dissimilar interfaces between

the embedded refractory particles and the Cu matrix appear in complete form-fitting contact for most cases. Only for larger refractory particles within a matrix of fine Cu particles, some gaps at dissimilar interfaces are observed.

This suggests that formation and bonding of these composites are mainly determined by the Cu matrix. In principle, the bonding between the refractory particles by adiabatic shear instabilities may be improved by higher process parameter sets. However, in practice, an increase of the process gas temperature would result in nozzle clogging by Cu. From the microstructures, it could not be distinguished whether the observed increase of Mo in the Mo-Cu composite coatings under higher process gas temperatures could be attributed to improved bonding of similar (Mo-Mo), dissimilar (Mo-Cu) refractory interfaces, or just better conditions for building up the Cu matrix (Cu-Cu). The isolated appearance of Mo-particles within the Cu matrix indicates that at least direct refractory bonds are rather rare.

The lack of similar refractory hard phase bonds has clear consequences on incorporating different particle sizes. Only hard phase particles that are similar or coarser than the soft Cu-component, result in a rather homogeneous phase distribution within the composite (compare Figure 4). If finer hard phase particles are used for the blend, these will only decorate the boundaries between the coarser soft ones building the matrix of the deposited composite. Hard-phase particles can only be incorporated into the composite coating at interfaces between soft-phase particles by getting trapped by secondary soft-phase particle impacts. Thus, geometric boundary conditions by particle sizes not only determine the composite homogeneity but also restrict the hard phase contents. The basic principles are similar for using coarse hard and small soft phase particles. A sufficiently high number of well bonded small soft phase particles is required to ensure trapping of the large hard phases. Thus, also the combination of large-hard and small-soft particles leads to reduction of the overall hard phase content.

4.2 Bonding at internal composite interfaces

The microstructural analyses only provide information about the dominant presence of dissimilar and soft-soft interfaces, but not about bonding types, nor their individual contributions to the composite properties. Therefore, mechanical testing and electrical conductivity measurements were used as complementary characterization techniques.

The tensile strength of the W-Cu composite, normalised with respect to the volume fraction of the soft matrix, remains constant with increasing the hard phase content (compare Figure 6). This implies that dissimilar interfaces (W-Cu) do not contribute to the overall cohesive strength, similar to that of the hard phase – hard phase (W-W) interfaces. Analysis of the fracture surfaces after testing supports this conclusion. Visible gaps between W and Cu particles in the as-sprayed state show that these interfaces are not metallurgically bonded. The refractory particles appear to be only form-fit embedded into the Cu matrix. The embedded W particles in this manner only reduce the load-bearing cross-section of the Cu matrix. The dissimilar interface situation does not improve by heat treatments. While the hard phase particles remain unchanged, the heat treatment softens the highly work hardened Cu matrix by recovery or recrystallization. Thus, the annealed composites have a lower strength than the as deposited ones. However, the thermal shrinkage of the matrix during cooling can cause a separation from the embedded refractory particles, with possibly associated plastic deformation providing risks of increased crack nuclei. The fracture surfaces after tensile testing (compare Figure 7) indicate wider cracks at the W-Cu interfaces at which coating failure might have been initiated. The situation is slightly

different for the Mo-Cu composite. Here, the normalised strength shows a slight increase with increasing the hard phase content. This indicates that at least parts of the dissimilar Mo-Cu interfaces are metallurgically bonded and contribute to the cohesive strength of the composite.

The mechanical tests demonstrate the minor role of dissimilar interfaces in the composite cohesion. Conductivity measurements, on the other hand, can be used to assess how tightly the refractory particles are embedded by the Cu matrix. The comparison of different circuit models (see Figure 8) reveals that, at least for W-Cu, the electrical conductivities of the cold gas sprayed composite coatings are best approximated by a parallel circuit model, i.e. by assuming a gap at the dissimilar interfaces (purple dashed curve in Figure 8). With the negligible current flow across the interface, the W particles contribute to conductivities in a similar manner as pores or insulators. Thus, it can be concluded that the Cu matrix and the embedded W particles already separate during the coating formation. The interface is not completely form-fit and in any case not bonded. Based on the present microstructures, commonly comprising isolated W particles in a Cu matrix, this can be explained as follows. When cooling down from the effective coating temperature during deposition to room temperature, Cu shrinks more than W. Presuming that the shear strength of the interfaces are lower than that of the bulk Cu, which should be the case in this system with clearly positive enthalpy of mixing, local separation will be likely to occur under certain loading conditions. According to the Wiedemann/Frantz rule [73], the electrical conductivity of metals scales directly with the thermal conductivity. Therefore, the embedded W will not contribute to the heat extraction in thermal management applications. For the Mo-Cu composites, the situation is not yet clear. In view of the scatter of data and comparatively low refractory contents, it cannot be excluded that some dissimilar interfaces stay bonded during cooling after deposition.

In order to achieve better agreement between the modeled curves and the measured values, the value for the conductivity of the Cu matrix σ_{Cu} was reduced to 71% IACS (International Annealed Copper Standard, conductivity of pure Cu, 58 MS/m [74]). This corresponds to 41.2 MS/m, although it should, for example, be about 82% IACS for a pure cold gas sprayed Cu coating in the as-sprayed state. This indicates that the impacts of refractory particles introduce more defects into the Cu matrix than in the build-up of pure, cold gas sprayed Cu coatings.

According to literature [75], the dislocation density has only minor influence on the conductivity of pure Cu. At a degree of 80% deformation, the conductivity only drops to 98% IACS. In contrast, even small amounts of impurity phases can significantly reduce the electrical conductivity, depending on the distribution in the crystal lattice. For example, dispersion-hardened Cu with 0.7% Al_2O_3 exhibits a conductivity of only 85% IACS. However, it is difficult to understand in what way refractory particles can lead to impurities in the Cu matrix. An alternative explanation could be provided by the existence of nano-scale persistent dislocation loops [14, 76-78]. The enhanced deformation by hitting hard phases or by following refractory particle impacts could initiate point defects over wider regions of the Cu matrix via cross-gliding, which condense as dislocation rings and act similarly to nanoscale precipitates.

To a certain extent, the build-up of composites by cold spraying can be explained by considering the interface chemistry. Table 5 compares the available data on the interface bonding in cold sprayed composite coatings, for mixtures of different powder materials [25], with the respective binary enthalpy of mixing. For negative enthalpies of mixing, such as for Ti-Al or Ni-Ti, an attractive chemical interaction occurs and the resulting composite coatings form a strong internal bond. Weak positive

enthalpies can still be compensated by contributions from the entropy of mixing and hence result in cohesion. However, in the case of strong positive enthalpies of mixing, such as for W-Cu, Mo-Cu or Cu-Cr, there is a repulsive interaction, hence the harder powder particles are merely embedded into the composite coating without forming a bond at the particle interfaces. Thus, apart from individual deformation behavior, the binary enthalpy of mixing of the composite materials defines an additional condition for successful composite formation by cold spraying.

		$\Delta H_{f\ M1\text{-}M2}$ [kJ/g-atom]**	Literature source	Rating of particle-particle bonding
W	Cu	+33	[64], this publication	Only embedded
Mo	Cu	+28	This publication	Only embedded
Ag	Ni	+23	[79]	Only embedded
Cu	Cr	+19	[80]	Only embedded
Al	Sn	+4 (2)	[81-83]	Bonded
Al	Zn	+4 (3)	[27, 84, 85]	Bonded
Cu	Ta	+3	[86]	Bonded
W	Ni	-5	[86]	Bonded
Cu	In	-7 (1)	[87]	Bonded
Ni	Cr	-10	[88-91]	Bonded
Fe	Al	-32	[92]	Bonded
Ni	Al	-48	[93-95]	Bonded
Ni	Ti	-52	[96]	Bonded
Ti	Al	-61	[97, 98]	Bonded

*Table 5: Cold sprayed composite coatings sorted by binary enthalpies of mixing and respective rating of internal coating cohesion [25]. (** Data for ΔH_f from [57], or alternatively (1): [99], (2): [100], (3): [101].)*

4.3 Consequences for the statistics of bonding probabilities

The window of deposition on the plane of particle temperature and velocity (see

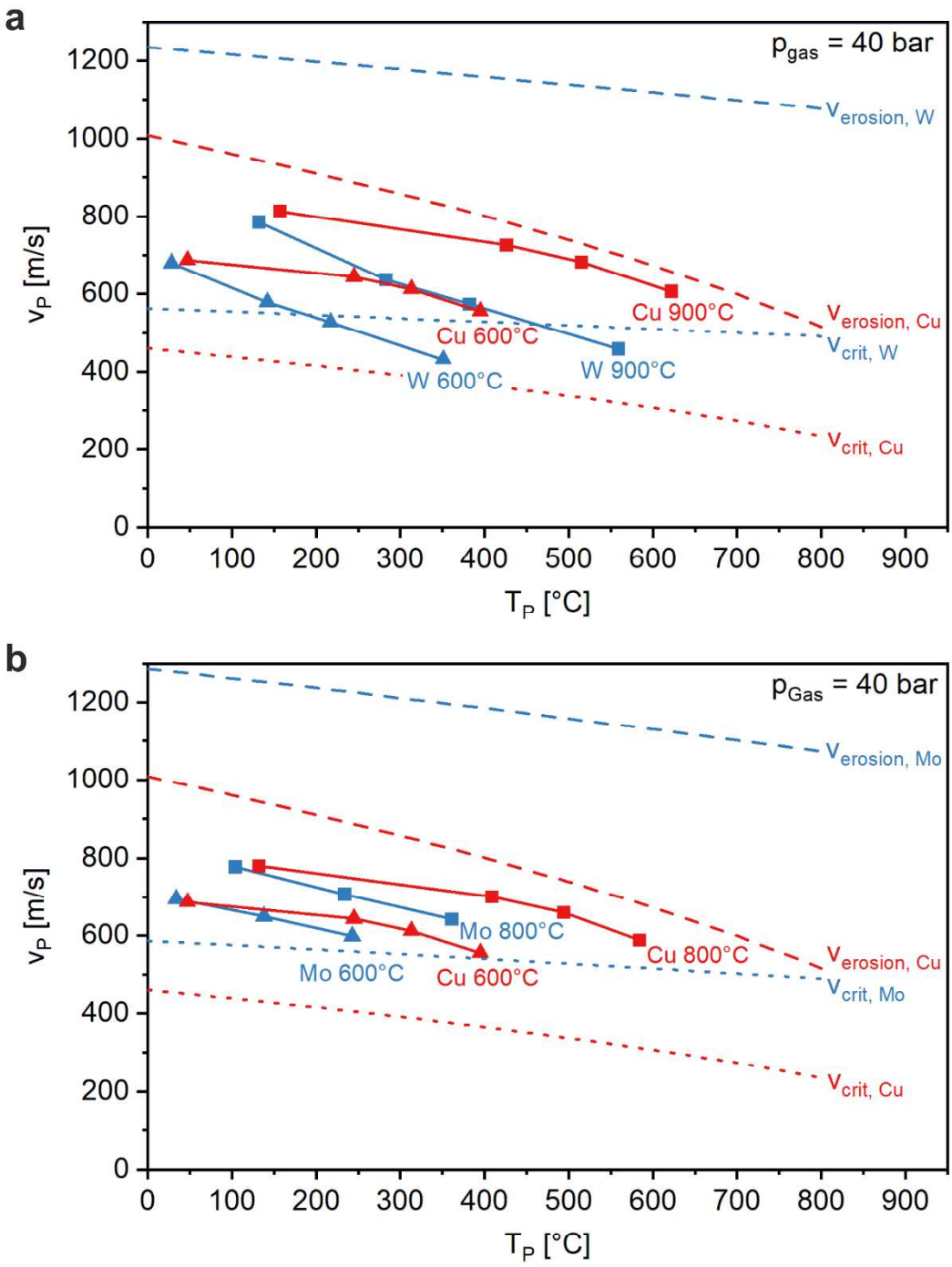

Figure 3), and the normalised impact velocity (i.e. the coating quality parameters η), can only provide information on the success of forming similar bonds. For instance, the low η values for the refractory particles indicate that similar bonding for these particles is unlikely to occur at the given spray parameter sets, whereas Cu particles could be well bonded together under the same conditions. However, the comparison does not supply any information about the quality of dissimilar bonds.

During formation of a composite, different impact scenarios, including a particle landing on an inhomogeneous surface, e.g. partly covered by Cu and partly by W, must be considered. Thus, local interfacial interactions, and the factors influencing these interactions (such as the particle size ratios,

particle size distributions and volume fractions of the constituents), must be included in the analytical descriptions of the composite build-up.

For example, for Cu on W impact events, it is conceivable that a large Cu particle hits a smaller W particle bonded within the matrix. In his scenario, the Cu will cover most of the W-particle embedding it in the layer. In this case, W-Cu bonds not necessarily have to contribute to cohesion since the flanks of the Cu particle could bond to the surrounding Cu matrix. The associated statistics for that will require Cu on the surface for covering the W particle. Such 3-particle interaction inevitably leads to lower amounts of finer W particles getting embedded into the composite coating. For example, using powders with 50 vol.% refractory content, only 5 vol.% W is incorporated into the W_{fine}-Cu_{coarse} composite coating, while 27 vol.% W is found in the corresponding W_{coarse}-Cu_{coarse} coating (compare Figure 5).

As described in methods, the parameters considering different surface coverages for hard-hard (B_{h-h}), soft-hard (B_{s-h}), as well as bonding probabilities hard-soft (H_{h-s}) and soft-soft (H_{s-s}) are determined by fitting procedures. Applying this statistical model to composite deposition allows to judge whether an impacting particle sticks to the surface or not, depending on the situation given by the constituents in the targeted area. By summing up over all impacts within the deposit volume, the model can describe the overall and individual deposition efficiencies (compare Figure 9 and Figure 10), based on which the fraction of refractory metals in the cold gas sprayed composites can be worked out.

In cold spraying of powder blends, a key objective is often to achieve a high hard phase content in the composite. The model provides a guideline to achieve this objective, e.g. by showing the main influences on the deposition efficiency of the hard phase, as given in Figure 9 and Figure 11. For instance, coarse particles of both constituents in the W-Cu system will result in the highest deposition efficiencies at high W fractions. In comparison, the use of fine / fine blends is less effective, probably due to the increased probabilities for W on W impacts. The deposition efficiency of the hard phases for all cases decreases monotonically with increasing the hard phase content. In agreement with the model, a deposition efficiency of DE_W = 3% was measured for a W_{fine}-Cu_{coarse} mixture, while the W_{coarse}-Cu_{coarse} mixture showed a deposition efficiency of DE_W = 35% (compare Figure 9). Similar trends are also reported in the literature [66]. Using Cu powders of d_{Cu} = 20 µm and d_{Cu} = 50 µm with W powder of d_W = 10 µm, the authors found a deposition efficiency of DE_W = 49% for the mixture with coarser Cu powder, whereas a slightly higher deposition efficiency of DE_W = 60% was obtained for the mixture with the finer Cu powder, the overall relatively high deposition efficiencies in that study being achieved by using He as process gas. Nevertheless, previous studies confirm that a powder blend with more similar particle size distributions of the components ensures a higher deposition efficiency. As expected, the use of fine soft phase and coarse hard phase particles, here (W_{coarse} –Cu_{fine}), results in the lowest deposition efficiencies of the hard phases.

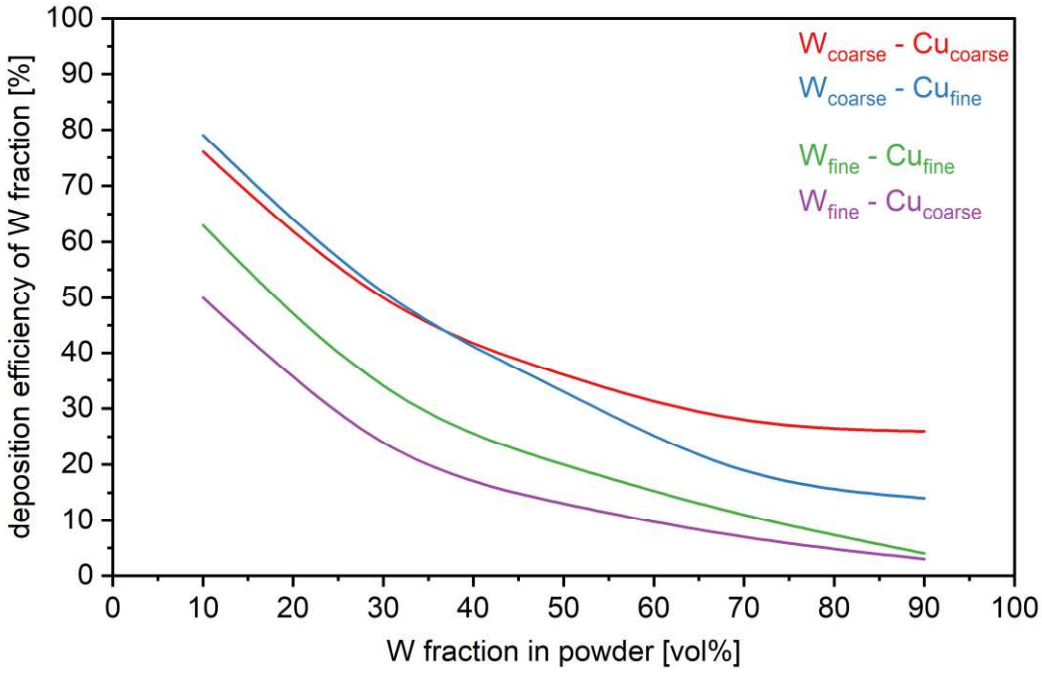

Figure 11: Simulated deposition efficiencies for the W fractions in different W-Cu powder blends. For high W contents in the powder, the blend W_{coarse}-Cu_{coarse} guarantees the overall highest DE_W. The blends with fine W powders result in comparatively low deposition efficiencies. The results were obtained with simulation parameters of $B_{W-W} = 0.05$, $B_{Cu-W} = 0.90$, $H_{W-Cu} = 1.00$, $H_{Cu-Cu} = 1.00$.

In the model, materials with less repulsive interactions would be represented by larger adhesion probabilities. Moreover, higher particle velocities or temperatures could increase the hard phase contents of the deposits, by increasing the overall η and thus deposition efficiencies. As shown for Mo-Cu (compare Figure 5), the Mo content in the cold sprayed composite coating rises with increased η-values. The same is true for the W –Cu blends. As reported in ref. [66], a high deposition efficiency of 60% was achieved for W by preheating the powders to ~600°C and using helium as process gas (p_{gas} = 29 bar and T_{Gas} = 500°C). Using the KSS software [10], the impact conditions for the W-particle are calculated to be as follows: v_P = 840 m/s, T_P = -92°C, η = 1.5. Such a high value of η should allow for W to W bonds. In addition, higher η-values for the soft phase causes a larger flattening ratio [15], hence a potentially larger area to which hard particles can bond.

In practice, mixtures that contain metallic and ceramic powders are more frequently used [40, 42, 44, 45, 47]. A suitable description should consider that the ceramic powders do not deform plastically. Only the softer, metallic matrix can provide the suitable conditions for the coating formation. Thus, the maximum attainable hard phase content stays rather low. Moreover, using higher parameter sets may cause more deformation of the metallic constituents and provide larger areas for bonding, hence leading to possible improvements, but also increasing the risk that ceramic particles fracture upon impact instead of contributing to composite formation.

Using literature data for the example of cold spraying an Al-Al_2O_3 powder mixture given in the work of Zhang et.al. [39], the possible application of the statistical model has here been tested for a ceramic – metal system by adjusting the parameters of critical coverage B and adhesion probability H. The authors used aluminum powder and aluminum oxide powder with sizes of d_{Al} = 10 µm and with d_{Al2O3} = 20 µm, respectively, in cold gas spraying and varied volume fractions in a range from 15 to 75 vol.% Al_2O_3. Reported data on deposition efficiencies and volume fractions of hard material in the generated

deposits were used as input parameters for the present simulation. The adhesion probability, i.e. the probability with which particles bond to a soft surface, were readjusted to 30 % for the case of Al_2O_3 on Al and to 50% and for Al on Al impacts. The comparison of experimental and modelling results in Figure 12 show a rather good agreement and demonstrate the applicability of the model for other types of material combination in cold spraying. Changing spray parameter sets to yield higher η-values improved cohesion of the aluminum matrix, but had no significant effect on the Al_2O_3 content in the sprayed layer. The discrepancies between the experimental data and the model for high Al_2O_3 contents of 75 vol. % might be attributed to peening effects and to flattening of previously impacted particles associated with larger, effective amounts of Al interfaces allowing for bonding, which is not included in the model yet.

A large number of examples can be found in the literature for the described trends for using powder mixtures of metallic and ceramic particles in cold spraying and respective limitations in reaching high hard phase contents in the deposited composite [24, 36, 38-42, 44, 45, 47]. The limited contribution to interface bonding is mainly attributed to the limited plastic deformation of the hard phases but also to the type of chemical interaction between soft and hard phases (as mentioned above in Section 4.2). We presume that dissimilar bonding probabilities can be improved by using higher η-values, and more attractive chemical interaction, or both, although none of the existing bonding criteria considers the chemical factor. Examples for enhanced spray conditions to give higher η values are already discussed above. An example for the type of interaction is given in literature for cold spraying of blends of Al with different hard phases as Al_2O_3, SiC or TiN [24]. The comparison shows that by more attractive chemical interaction, the use of SiC or TiN ensure higher hard phase contents than attainable by using Al_2O_3.

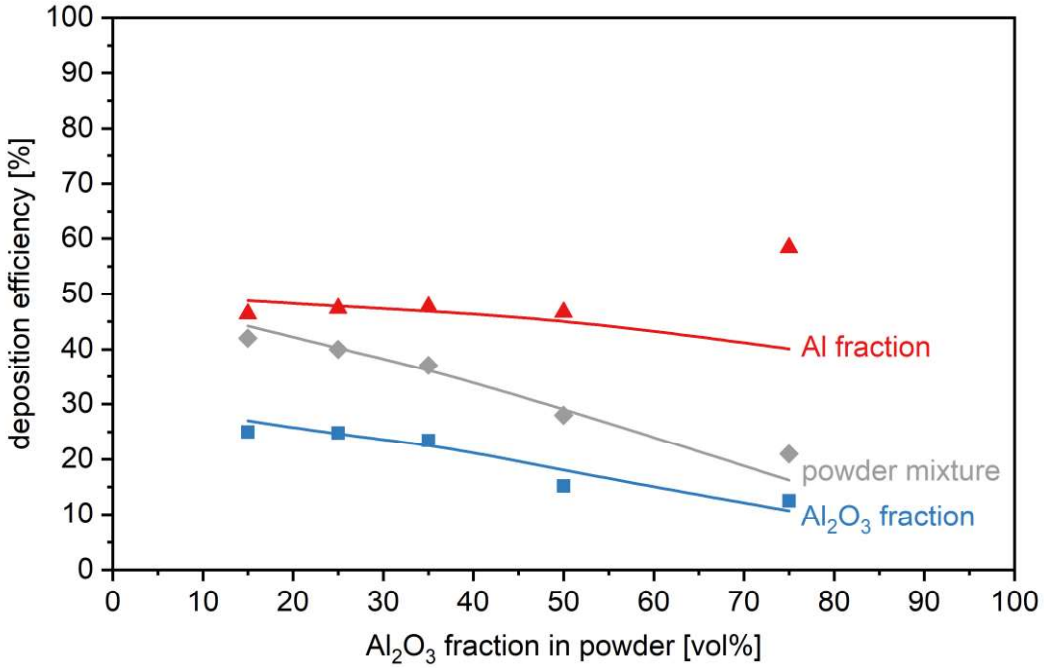

Figure 12: Comparison of simulated and experimentally determined deposition efficiencies for cold gas sprayed Al-Al_2O_3 powder mixtures given in literature [39]. Up to a volume fraction of 50% Al_2O_3 in the powder, the statistical model reproduces the observed deposition efficiencies. $B_{Al2O3\text{-}Al2O3}$ = 0.15, $B_{Al\text{-}Al2O3}$ = 0.70, $H_{Al2O3\text{-}Al}$ = 0.30, $H_{Al\text{-}Al}$ = 0.50.

4.4 Forecast for describing general trends

In principle, most of the influences for the success in cold spraying can be understood on the basis of individual impact statistics and respective particle – surface interaction. Individual probabilities contain attainable η-values, temperature dependent surface deformability as well as types of chemical interaction or possible mixed states given at the target surface to describe bonding success. Summing up over multiple events can then describe layer build-up. Such a statistical model including individual interaction has the charm to reach a more general description of cold spraying.

So far, for cold spraying of metal alloys, the impact velocity to critical velocity ratios η provide already a good estimate for attainable deposit properties, in the background assuming uniform interaction parameters. However, even for this situation, the interaction could be non-uniform. Individually different powders sizes of a given batch and attained impact conditions (v_p, T_p) could results in different η-values [2]. The deposit quality is then determined by the contributions of all different interactions and thus bonding probabilities. Similar is given by effective surface temperatures that define the amount of shear instabilities on the deposit surface as additional support for bonding of the impacting particle [17].

A key issue might concern building up the first layer on the substrate or part to coat. At first instance, bonding is determined by the plasticity of the substrate surface and the deposit material and abilities to form common interfaces by adiabatic shear instabilities [22]. For different properties of both, it would be beneficial to modify the surface topography to enable trapping of areas of shear instabilities to enhance amounts of common interfaces for optimum adhesion. At second instance, particularly in case of rather rigid substrates, chemical interactions could dominate. For example, results shown by Drehmann et.al. for cold spraying of (pure) aluminum onto different ceramic substrate materials revealed that the coating adhesion on SiC is higher than that on Al_2O_3 substrates [20, 102-104]. Other hints on chemical influences are given by results for cold spraying onto rigid Cr-layers. Differences between bonded Al and non-bonded Cu are explained by attractive or repulsive chemical interaction, respectively [86]. In principle, all that could be summarized in first layer specific interaction parameters within a statistical model.

At this point, the presented use of bonding probabilities for describing coating formation in cold spraying should be seen as a first attempt to demonstrate the capabilities of such an approach. More efforts are needed to calibrate the parameters for surface coverage and interaction. Such should include individually η -dependent flattening ratios [15], a description for effective amounts of areas of shear instability in contact, and information about interface chemistry. If explored in detail, such models could describe adhesion to different material types, the influence of surface temperature on layer quality, building-up of metallic alloy deposits where different η -values could be expected by particle size dependent powder strengths or impact conditions, as well as the formation of composites.

5. Summary and conclusions

Taking W – Cu and Mo – Cu as model systems for depositing composite coatings by cold spraying of powder blends, general features were investigated that determine attainable hard phase contents. By using a variety of different initial compositions, rather dense and well adhering deposits are obtained. However, composite properties like mechanical strength and electrical conductivity are mainly determined by the Cu matrix, due to non-sufficient bonding of the embedded, isolated hard refractory

W-particles. The deposition efficiencies of the hard phases decrease with increasing hard phase contents and are highest for using similar hard and soft phase powder sizes. To certain extent, the hard phase contents can be increased by using spray parameter sets that correspond to higher impact to critical velocity ratios η. However, whatever the spray conditions are, the hard phase contents of the composite will run into a saturation regime for high amounts being in the initial blends. By circuit models for the conductivity, it could be demonstrated that the refractory phases stay loosely, not even form-fit bonded within the matrix.

The application of a statistical model dealing with parameters of surface coverage and individual bonding probabilities enables to distinguish influences by hard phase contents and powder sizes on individual deposition efficiencies.

The main conclusions for cold spraying of powder blends can be summarized as following:

- Attainable hard phase contents are determined by impact statistics and individual bonding probabilities.
- Parameters for surface coverage for ensuring max. deposition are meet only at similar sizes of hard and soft phase powders.
- Individual similar or dissimilar interaction during impact can be described by bonding probabilities.
- The bonding probabilities increase with higher impact to critical velocity ratios η and more attractive chemical interaction.

The amount of refractory metal is largely determined by the impact statistics and the boundary conditions for bonding (adhesion probability), given here by the chemistry of the composite components and the spraying conditions (η-value). For the spray parameters and material combinations used in this work, impact events of a hard material particle onto an already deposited hard material particle did not result in adhesion.

The phenomena and coating properties discussed can also be qualitatively transferred to cold spraying of other powder mixtures, in which one of the partners does not deform or does not or only barely bond, such as in low-pressure cold gas spraying of Cu with aluminum oxide particles. Similar is valid for combinations of materials, which show repulsive chemical interaction.

Thus, in summary the applied methods and particularly the statistical model prove to be powerful tools for describing the formation of composites by cold spraying of powder blends, which could also be transferred to other material systems. The identification of individual contributions by plastic deformation and interface chemistry may even allow for further generalization in the description of cold spraying.

Acknowledgements

This work was partly financed by the program “InnoNet”, grand no. 16IN0695, of the Federal Ministry of Economics and Technology. The authors also like to thank the team from HSU for technical support

and fruitful discussions, here in alphabetical order namely Thomas Breckwoldt, Herbert Hübner, Heinz-Dieter Müller, Norbert Németh, Camilla Schulze, Matthias Schulze and Uwe Wagener.

Supplements

Table 6: Electrical conductivities of W-Cu and Mo-Cu composite bulk materials according to literature

W-Cu:							
wt-% Cu	wt-% W	vol-% Cu	vol-% W	resistivity [ohm*cm]	conductivity [MS/m]	Material description	Literature source
30	70	48.1	51.9	0.00000400	25.0	H.C. Starck WCu 70/30 Tungsten-Copper Composite Material	https://www.matweb.com/search/DataSheet.aspx?MatGUID=33797517d78141d0a9443beb3d69dcb9
25	75	41.9	58.1	0.00000470	21.3	H.C. Starck WCu 75/25 Tungsten-Copper Composite Material	https://www.matweb.com/search/DataSheet.aspx?MatGUID=8e386323751446cab53e1d834006d7a8
20	80	35.1	64.9	0.00000500	20.0	H.C. Starck WCu 80/20 Tungsten-Copper Composite Material	https://www.matweb.com/search/DataSheet.aspx?MatGUID=e1978f27bcb94ac7b71c126d9ce25c92
15	85	27.6	72.4	0.00000500	20.0	H.C. Starck WCu 85/15 Tungsten-Copper Composite Material	https://www.matweb.com/search/DataSheet.aspx?MatGUID=3a69717d7a154c5d95333d2858d298cb
10	90	19.4	80.6	0.00000520	19.2	H.C. Starck WCu 90/10 Tungsten-Copper Composite Material	https://www.matweb.com/search/DataSheet.aspx?MatGUID=5d19bc1cf7e3474788db0b6dbfc08cca
45	55	63.9	36.1	0.00000300	33.3	Hogen Duralloy H1W 55Tungsten/45Copper PM Metal composite	https://www.matweb.com/search/DataSheet.aspx?MatGUID=cb7c59739b424132869283738adf8e28&ckck=1
20	80	35.1	64.9	0.00000421	23.8	CMW® ELKONITE® 30W3 Infiltrated Copper Tungsten contact material ASTM B702, Class E, infiltrated, RWMA Class 12	https://www.matweb.com/search/DataSheet.aspx?MatGUID=a64b100b129e4cb696907f6f3f703fd5
30	70	48.1	51.9	0.00000359	27.9	CMW® ELKONITE® 5W3 Tungsten Copper material ASTM B702, Class C, infiltrated	https://www.matweb.com/search/DataSheet.aspx?MatGUID=e3bdf3fb38c549c4a96bfe972065c53c
45	55	63.9	36.1	0.00000325	30.8	CMW® ELKONITE® 1W3 Copper Tungsten RWMA Class 10	https://www.matweb.com/search/DataSheet.aspx?MatGUID=9ae3384939e44d3a9024902c81488030
45	55	63.9	36.1	0.00000300	33.3	Mi-Tech Metals CW55 55 Tungsten/45 Copper PM Metal Composite	https://www.matweb.com/search/DataSheet.aspx?MatGUID=577e84766c3442e0860f0c4e91ff5157
32	68	50.4	49.6	0.00000340	29.4	Mi-Tech Metals CW68 68 Tungsten/32 Copper PM Metal Composite	https://www.matweb.com/search/DataSheet.aspx?MatGUID=d57afd7b003e49d0a75cbd72e7c636c9
30	70	48.1	51.9	0.00000350	28.6	Mi-Tech Metals CW70 70 Tungsten/30 Copper PM Metal Composite	https://www.matweb.com/search/DataSheet.aspx?MatGUID=7b6ac6d5463e4a6ea240bcccc3221df5
20	80	35.1	64.9	0.00000380	26.3	Mi-Tech Metals CW80 80 Tungsten/20 Copper PM Metal Composite	https://www.matweb.com/search/DataSheet.aspx?MatGUID=f33f637e9b84488e80ecd1b6bae297ad

10	90	19.4	80.6	0.00000493	20.3	CMW® THERMKON® 62 Tungsten Copper parts	https://www.matweb.com/search/DataSheet.aspx?MatGUID=f10331bcad9041599aa81399595e8401
15	85	27.6	72.4	0.00000493	20.3	CMW® THERMKON® 68 Tungsten Copper parts	https://www.matweb.com/search/DataSheet.aspx?MatGUID=6886ab79f57b459cb6b42ec96d8f4816
20	80	35.1	64.9	0.00000466	21.5	CMW® THERMKON® 76 Tungsten Copper parts	https://www.matweb.com/search/DataSheet.aspx?MatGUID=2d0bdf67743d4e9eb53e244e90b76682
25	75	41.9	58.1	0.00000383	26.1	CMW® THERMKON® 83 Tungsten Copper parts	https://www.matweb.com/search/DataSheet.aspx?MatGUID=74fd544fbdca4ba09812425cdb9acbed
Mo-Cu:							
wt-% Cu	wt-% Mo	vol-% Cu	vol-% Mo	resistivity [ohm*cm]	conductivity [MS/m]		
35	65	38.1	61.9	0.00000400	25.0	H.C. Starck MoCu 65/35 Molybdenum-Copper Composite Material	https://www.matweb.com/search/DataSheet.aspx?MatGUID=9e50dc2b40884427a023f7adf119047f
30	70	32.9	67.1	0.00000380	26.3	H.C. Starck MoCu 70/30 Molybdenum-Copper Composite Material	https://www.matweb.com/search/DataSheet.aspx?MatGUID=cc7ba834c8aa4aed9e6e8f67380cec2f
20	80	22.2	77.8	0.00000420	23.8	H.C. Starck MoCu 80/20 Molybdenum-Copper Composite Material	https://www.matweb.com/search/DataSheet.aspx?MatGUID=2bd78c0dafc94a29a38875abec85501e
15	85	16.8	83.2	0.00000420	23.8	H.C. Starck MoCu 85/15 Molybdenum-Copper Composite Material	https://www.matweb.com/search/DataSheet.aspx?MatGUID=6d81f3c056564191ba07f740acb194f9
20	80	22.2	77.8	0.00000539	18.6	CMW® THERMKON® 70M Molybdenum Copper parts	https://www.matweb.com/search/DataSheet.aspx?MatGUID=bb0b4240912f4ba29fbca241881a4a86
15	85	16.8	83.2	0.00000616	16.2	CMW® THERMKON® 65M Molybdenum Copper parts	https://www.matweb.com/search/DataSheet.aspx?MatGUID=ba42fc76962b4fe1a585664549a03d08

Data availability

The raw/processed data required to reproduce these findings cannot be shared at this time as the data also forms part of an ongoing study.

References

1. Assadi, H., et al., *Cold spraying–a materials perspective.* Acta Materialia, 2016. **116**: p. 382-407.
2. *High Pressure Cold Spray: Principles and Applications*, ed. C.M. Kay and J. Karthikeyan. 2016, Ohio, USA: ASM International.
3. Raoelison, R.N., et al., *Cold gas dynamic spray technology: A comprehensive review of processing conditions for various technological developments till to date.* Additive Manufacturing, 2018. **19**: p. 134-159.
4. Papyrin, A., et al., *Cold spray technology*. 2006: Elsevier.
5. Villafuerte, J., *Modern cold spray: materials, process, and applications*. 2015: Springer.
6. Champagne, V.K., *The cold spray materials deposition process*. 2007: Elsevier.
7. Stoltenhoff, T., H. Kreye, and H.J. Richter, *An analysis of the cold spray process and its coatings.* Journal of Thermal Spray Technology, 2002. **11**(4): p. 542-550.
8. Stoltenhoff, T., *Kaltgasspritzen von Kupfer - Eine strömungsmechanische und werkstoffkundliche Analyse und Optimierung des Spritzprozesses*. 2004, Aachen: Shaker Verlag.
9. Assadi, H., et al., *Bonding mechanism in cold gas spraying.* Acta Materialia, 2003. **51**(15): p. 4379-4394.
10. *KSS software package*. 2018, Kinetic Spray Solutions GmbH.
11. Gärtner, F., et al., *The cold spray process and its potential for industrial applications.* Journal of Thermal Spray Technology, 2006. **15**(2): p. 223-232.
12. McCune, R.C., et al., *Characterization of copper layers produced by cold gas-dynamic spraying.* Journal of Thermal Spray Technology, 2000. **9**(1): p. 73-82.
13. Schmidt, T., et al., *Development of a generalized parameter window for cold spray deposition.* Acta Materialia, 2006. **54**(3): p. 729-742.
14. Stoltenhoff, T., et al., *Microstructures and key properties of cold-sprayed and thermally sprayed copper coatings.* Surface & Coatings Technology, 2006. **200**(16-17): p. 4947-4960.
15. Assadi, H., et al., *On parameter selection in cold spraying.* Journal of thermal spray technology, 2011. **20**(6): p. 1161-1176.
16. Vidaller, M.V., et al., *Single Impact Bonding of Cold Sprayed Ti-6Al-4V Powders on Different Substrates.* Journal of Thermal Spray Technology, 2015. **24**(4): p. 644-658.
17. Arabgol, Z., et al., *Influence of thermal properties and temperature of substrate on the quality of cold-sprayed deposits.* Acta Materialia, 2017. **127**: p. 287-301.
18. Donner, K.R., F. Gärtner, and T. Klassen, *Metallization of Thin Al_2O_3 Layers in Power Electronics Using Cold Gas Spraying.* Journal of Thermal Spray Technology, 2011. **20**(1): p. 299-306.
19. Ernst, K.-R., et al., *Effect of substrate temperature on cold-gas-sprayed coatings on ceramic substrates.* Journal of thermal spray technology, 2013. **22**(2-3): p. 422-432.
20. Drehmann, R., et al., *Splat formation and adhesion mechanisms of cold gas-sprayed Al coatings on Al_2O_3 substrates.* Journal of Thermal Spray Technology, 2014. **23**(1-2): p. 68-75.
21. Drehmann, R., et al., *Essential factors influencing the bonding strength of cold-sprayed aluminum coatings on ceramic substrates.* Journal of Thermal Spray Technology, 2018. **27**(3): p. 446-455.
22. Theimer, S., et al., *Optimization Adhesion in Cold Spraying onto Hard Substrates: A Case Study for Brass Coatings.* Journal of Thermal Spray Technology, 2019. **28**(1): p. 124-134.
23. Davis, J.R., *Handbook of thermal spray technology*. 2004: ASM international.
24. Yu, M. and W. Li, *Metal Matrix Composite Coatings by Cold Spray*, in *Cold-Spray Coatings: Recent Trends and Future perspectives*, P. Cavaliere, Editor. 2018, Springer International Publishing: Cham. p. 297-318.
25. Li, W., et al., *A Review of Advanced Composite and Nanostructured Coatings by Solid-State Cold Spraying Process.* Critical Reviews in Solid State and Materials Sciences, 2018: p. 1-48.

26. Lee, Y.T.R., et al., *Cold-Sprayed Metal Matrix Composite Coatings*, in *Cold-Spray Coatings*. 2018, Springer. p. 275-295.
27. Zhou, X., et al., *Deposition behavior of mixed binary metallic powders in cold spraying process.* Applied Surface Science, 2011. **257**(24): p. 10628-10633.
28. Kikuchi, S., et al., *Microstructures and thermal properties of cold-sprayed Cu-Cr composite coatings.* Journal of thermal spray technology, 2013. **22**(6): p. 926-931.
29. Maestracci, R., et al., *Deposition of composite coatings by cold spray using stainless steel 316L, copper and Tribaloy T-700 powder mixtures.* Surface and Coatings Technology, 2016. **287**: p. 1-8.
30. Nikbakht, R., et al., *Asymmetrical bonding in cold spraying of dissimilar materials.* Applied Surface Science, 2018. **444**: p. 621-632.
31. Nikbakht, R., H. Assadi, and B. Jodoin, *Intermetallic phase evolution of cold-sprayed Ni-Ti composite coatings: influence of as-sprayed chemical composition.* Journal of Thermal Spray Technology, 2021. **30**(1): p. 119-130.
32. Maev, R.G. and V. Leshchynsky, *Air gas dynamic spraying of powder mixtures: Theory and application.* Journal of Thermal Spray Technology, 2006. **15**(2): p. 198-205.
33. Bu, H., et al., *Cold spray blended Al+ Mg17Al12 coating for corrosion protection of AZ91D magnesium alloy.* Surface and Coatings Technology, 2012. **207**: p. 155-162.
34. Cizek, J., et al., *Oxidation performance of cold spray Ti–Al barrier coated γ-TiAl intermetallic substrates.* Surface and Coatings Technology, 2015. **268**: p. 85-89.
35. Klinkov, S.V., et al., *Deposition of multicomponent coatings by Cold Spray.* Surface & Coatings Technology, 2008. **202**(24): p. 5858-5862.
36. Pantelis, D., et al. *Microstructural study of copper and copper/alumina composite coatings produced by cold spray process*. in *Advanced Materials Research*. 2010. Trans Tech Publ.
37. Lee, H.Y., et al., *Correlation between Al_2O_3 particles and interface of Al–Al_2O_3 coatings by cold spray.* Applied surface science, 2005. **252**(5): p. 1891-1898.
38. Spencer, K., D. Fabijanic, and M.-X. Zhang, *The use of Al–Al_2O_3 cold spray coatings to improve the surface properties of magnesium alloys.* Surface and Coatings Technology, 2009. **204**(3): p. 336-344.
39. Wang, Q.A., et al., *The influence of ceramic particles on bond strength of cold spray composite coatings on AZ91 alloy substrate.* Surface & Coatings Technology, 2010. **205**(1): p. 50-56.
40. Hodder, K., et al., *Fabrication of aluminum–alumina metal matrix composites via cold gas dynamic spraying at low pressure followed by friction stir processing.* Materials Science and Engineering: A, 2012. **556**: p. 114-121.
41. Heimann, R.B., et al., *High-pressure cold gas dynamic (CGD)-sprayed alumina-reinforced aluminum coatings for potential application as space construction material.* Surface and Coatings Technology, 2014. **252**: p. 113-119.
42. Hodder, K., J. Nychka, and A. McDonald, *Comparison of 10 μm and 20 nm Al-Al_2O_3 metal matrix composite coatings fabricated by low-pressure cold gas dynamic spraying.* Journal of Thermal Spray Technology, 2014. **23**(5): p. 839-848.
43. Shockley, J., et al., *The influence of Al_2O_3 particle morphology on the coating formation and dry sliding wear behavior of cold sprayed Al–Al_2O_3 composites.* Surface and Coatings Technology, 2015. **270**: p. 324-333.
44. Koivuluoto, H., et al., *Microstructure and Mechanical Properties of Low-Pressure Cold-Sprayed (LPCS) Coatings.* Journal of Thermal Spray Technology, 2008. **17**(5): p. 721-727.
45. Koivuluoto, H. and P. Vuoristo, *Effect of Powder Type and Composition on Structure and Mechanical Properties of Cu + Al_2O_3 Coatings Prepared by using Low-Pressure Cold Spray Process.* Journal of Thermal Spray Technology, 2010: p. 1-12.
46. Miguel, J., J. Guilemany, and S. Dosta, *Effect of the spraying process on the microstructure and tribological properties of bronze–alumina composite coatings.* Surface and Coatings Technology, 2010. **205**(7): p. 2184-2190.

47. Koivuluoto, H., et al., *High Pressure Cold Sprayed (HPCS) and Low Pressure Cold Sprayed (LPCS) Coatings Prepared from OFHC Cu Feedstock: Overview from Powder Characteristics to Coating Properties.* Journal of Thermal Spray Technology, 2012. **21**(5): p. 1065-1075.
48. Triantou, K.I., et al., *Microstructure and tribological behavior of copper and composite copper+ alumina cold sprayed coatings for various alumina contents.* Wear, 2015. **336**: p. 96-107.
49. Lee, H.Y., et al., *Cold spray of SiC and Al_2O_3 with soft metal incorporation: A technical contribution.* Journal of Thermal Spray Technology, 2004. **13**(2): p. 184-189.
50. Sansoucy, E., et al., *Properties of SiC-reinforced aluminum alloy coatings produced by the cold gas dynamic spraying process.* Surface & Coatings Technology, 2008. **202**(16): p. 3988-3996.
51. Yandouzi, M., P. Richer, and B. Jodoin, *SiC particulate reinforced Al-12Si alloy composite coatings produced by the pulsed gas dynamic spray process: Microstructure and properties.* Surface & Coatings Technology, 2009. **203**(20-21): p. 3260-3270.
52. Yu, M., et al., *Microstructure, mechanical property and wear performance of cold sprayed Al5056/SiCp composite coatings: effect of reinforcement content.* Applied Surface Science, 2014. **289**: p. 188-196.
53. Yu, M., et al., *Effect of matrix/reinforcement combination on cold sprayed coating deposition behaviour.* Surface Engineering, 2014. **30**(11): p. 796-800.
54. Klinkov, S. and V. Kosarev, *Monte Carlo simulation of the Cold Spray process of mixtures of metal and ceramic powders.* Journal of Thermal Spray Technology, 2021. **30**(4): p. 1081-1092.
55. Fernandez, R. and B. Jodoin, *Cold spray aluminum–alumina cermet coatings: effect of alumina content.* Journal of thermal spray technology, 2018. **27**(4): p. 603-623.
56. Fernandez, R. and B. Jodoin, *Cold spray aluminum–alumina cermet coatings: effect of alumina morphology.* Journal of Thermal Spray Technology, 2019. **28**(4): p. 737-755.
57. De Boer, F.R., et al., *Cohesion in metals*. 1988.
58. www.matweb.com. 29.05.2021].
59. Pintsuk, G., et al., *Fabrication and characterization of vacuum plasma sprayed W/Cu-composites for extreme thermal conditions.* Journal of Materials Science, 2007. **42**(1): p. 30-39.
60. Döring, J.E., et al., *The processing of vacuum plasma-sprayed tungsten–copper composite coatings for high heat flux components.* Fusion Engineering and Design, 2003. **66-68**: p. 259-263.
61. Kang, H.-K. and S. Bong Kang, *Effect of feedstock injection methods on oxidation behavior and microstructure of plasma sprayed W/Cu composites.* Surface and Coatings Technology, 2004. **182**(1): p. 124-130.
62. Matějíček, J., et al. *Development and Properties of Tungsten-Based Coatings Sprayed by WSP (R)*. in *International Thermal Spray Conference, Basel, Switzerland*. 2005.
63. Matějíček, J., et al., *Copper-tungsten composites sprayed by HVOF.* Journal of Thermal Spray Technology, 2008. **17**(2): p. 177-180.
64. Kang, H.-K. and S.B. Kang, *Tungsten/copper composite deposits produced by a cold spray.* Scripta Materialia, 2003. **49**(12): p. 1169-1174.
65. Hall, A.C., et al., *Deposition Behavior in Cold Sprayed Copper-Tungsten Metal Matrix Composites*. 2015, Sandia National Lab.(SNL-NM), Albuquerque, NM (United States).
66. Shin, S., et al., *Effect of particle parameters on the deposition characteristics of a hard/soft-particles composite in kinetic spraying.* Surface & Coatings Technology, 2006. **201**(6): p. 3457-3461.
67. Schmidt, T., *Kaltgasspritzen: Eine Analyse des Materialverhaltens beim Partikelaufprall und die daraus abgeleitete Prozessoptimierung*. 2007: Shaker.
68. Schmidt, T., F. Gärtner, and H. Kreye, *New developments in cold spray based on higher gas and particle temperatures.* Journal of Thermal Spray Technology, 2006. **15**(4): p. 488-494.
69. Callister, W.D. and D.G. Rethwisch, *Materialwissenschaften und Werkstofftechnik: Eine Einführung*. 2012: John Wiley & Sons.
70. Gottstein, G., *Physikalische Grundlagen der Materialkunde*. 2007: Springer-Verlag.
71. Fuhrmann, E., *Einführung in die Werkstoffkunde und Werkstoffprüfung*. Vol. 2. 2008: expert verlag.

72. Bargel, H.-J. and G. Schulze, *Werkstoffkunde*. 2008: Springer-Verlag.
73. Franz, R. and G. Wiedemann, *Ueber die Wärme-Leitungsfähigkeit der Metalle.* Annalen der Physik, 1853. **165**(8): p. 497-531.
74. Standards, B., *Copper Wire Tables: Circular of the Bureau of Standards No. 31*. 1914, Government Printing Office Washington, DC.
75. Askeland, D.R. and P.P. Phulé, *The science and engineering of materials*. 2006: Springer.
76. Borchers, C., et al., *Formation of persistent dislocation loops by ultra-high strain-rate deformation during cold spraying.* Acta Materialia, 2005. **53**(10): p. 2991-3000.
77. Borchers, C., et al., *Microstructural bonding features of cold sprayed face centered cubic metals.* Journal of Applied Physics, 2004. **96**(8): p. 4288-4292.
78. Borchers, C., et al., *Microstructural and macroscopic properties of cold sprayed copper coatings.* Journal of Applied Physics, 2003. **93**(12): p. 10064-10070.
79. Rolland, G., et al., *Damage study of cold-sprayed composite materials for application to electrical contacts.* Journal of thermal spray technology, 2012. **21**(5): p. 758-772.
80. Wu, X.-k., et al., *Deposition behavior and characteristics of cold-sprayed Cu-Cr composite deposits.* Journal of thermal spray technology, 2012. **21**(5): p. 792-799.
81. Li, W.-Y., C.-J. Li, and G.-J. Yang, *Effect of impact-induced melting on interface microstructure and bonding of cold-sprayed zinc coating.* Applied Surface Science, 2010. **257**(5): p. 1516-1523.
82. Ning, X.-J., et al., *Cold spraying of Al–Sn binary alloy: Coating characteristics and particle bonding features.* Surface and Coatings Technology, 2008. **202**(9): p. 1681-1687.
83. Ning, X.-J., et al., *Characteristics and heat treatment of cold-sprayed Al–Sn binary alloy coatings.* Applied Surface Science, 2009. **255**(7): p. 3933-3939.
84. Zhao, Z.B., B. Gillispie, and J. Smith, *Coating deposition by the kinetic spray process.* Surface and Coatings Technology, 2006. **200**(16-17): p. 4746-4754.
85. Haixiang, L., et al., *Corrosion resistance of cold-sprayed Zn-50Al coatings in seawater.* Journal of Chinese Society for Corrosion and protection, 2010. **30**(1): p. 62-66.
86. Ernst, K.R., *Kaltgasspritzen für die Leistungselektronik*. 2021, Universitätsbibliothek der HSU/UniBwH.
87. Jin, Y.-M., et al., *Manufacturing and macroscopic properties of cold sprayed Cu-In coating material for sputtering target.* Journal of thermal spray technology, 2011. **20**(3): p. 497-507.
88. Bala, N., H. Singh, and S. Prakash, *Characterization and high-temperature oxidation behavior of cold-sprayed Ni-20Cr and Ni-50Cr coatings on boiler steels.* Metallurgical and Materials Transactions A, 2011. **42**(11): p. 3399-3416.
89. Bala, N., H. Singh, and S. Prakash, *High temperature corrosion behavior of cold spray Ni-20Cr coating on boiler steel in molten salt environment at 900 C.* Journal of Thermal Spray Technology, 2010. **19**(1-2): p. 110-118.
90. Singh, H., et al., *Evaluation of characteristics and behavior of cold sprayed Ni–20Cr coating at elevated temperature in waste incinerator plant.* Surface and Coatings Technology, 2015. **261**: p. 375-384.
91. Singh, H., et al., *Hot Corrosion Behavior of Cold-Sprayed Ni-50Cr Coating in an Incinerator Environment at 900 C.* Journal of Thermal Spray Technology, 2015. **24**(3): p. 570-578.
92. Wang, H.-T., et al., *Cold spraying of Fe/Al powder mixture: Coating characteristics and influence of heat treatment on the phase structure.* Applied Surface Science, 2008. **255**(5): p. 2538-2544.
93. Lee, H.Y., et al., *Alloying of cold-sprayed Al–Ni composite coatings by post-annealing.* Applied surface science, 2007. **253**(7): p. 3496-3502.
94. Lee, H.Y., et al., *Fabrication of cold sprayed Al-intermetallic compounds coatings by post annealing.* Materials Science and Engineering a-Structural Materials Properties Microstructure and Processing, 2006. **433**(1-2): p. 139-143.
95. Spencer, K. and M.X. Zhang, *The use of kinetic metallization to form intermetallic reinforced composite coatings by post-spray heat treatment.* Surface & Coatings Technology, 2009. **203**(20-21): p. 3019-3025.
96. Tria, S., et al., *Ball milled Ni–Ti powder deposited by cold spraying.* Journal of alloys and Compounds, 2009. **483**(1-2): p. 334-336.

97. Novoselova, T., et al., *Experimental study of titanium/aluminium deposits produced by cold gas dynamic spray.* Surface & Coatings Technology, 2006. **200**(8): p. 2775-2783.
98. Novoselova, T., et al., *Formation of TiAl intermetallics by heat treatment of cold-sprayed precursor deposits.* Journal of Alloys and Compounds, 2007. **436**(1-2): p. 69-77.
99. Muzzillo, C.P., C.E. Campbell, and T.J. Anderson, *Cu–Ga–In thermodynamics: experimental study, modeling, and implications for photovoltaics.* Journal of Materials Science, 2016. **51**(7): p. 3362-3379.
100. Waseda, Y., K.T. Jacob, and S. Tamaki, *Heat of Mixing and Activities in Liquid Al-Sn Alloys.* Zeitschrift für Naturforschung A, 1979. **34**(3): p. 320.
101. Murray, J.L., *The Al–Zn (Aluminum-Zinc) system.* Bulletin of Alloy Phase Diagrams, 1983. **4**(1): p. 55-73.
102. Drehmann, R., et al. *Essential factors influencing the bonding strength of cold sprayed aluminum coatings on ceramic substrates*. in *International Thermal Spray Conference*. 2017. Düsseldorf: DVS.
103. Drehmann, R., et al., *Interface characterization and bonding mechanisms of cold gas-sprayed Al coatings on ceramic substrates.* Journal of Thermal Spray Technology, 2015. **24**(1-2): p. 92-99.
104. Drehmann, R., et al. *Investigation of the Bonding Mechanisms of Al Coatings on Ceramic Substrates Deposited by Cold Gas Spraying and Magnetron Sputtering*. in *Proceedings International Thermal Spray Conference*. 2015.

Declaration of Competing Interest

Declaration of interests

☐The authors declare that they have no known competing financial interests or personal relationships that could have appeared to influence the work reported in this paper.

☒The authors declare the following financial interests/personal relationships which may be considered as potential competing interests:

Kerstin Raffaela Ernst reports a relationship with Oerlikon Coating Services GmbH that includes: employment.